AD-A146 229 ANALYSIS OF IN-PLANE AND OUT-OF-PLANE GROUND MOTIONS USING THE BOUNDARY E..(U) RHODE ISLAND UNIV KINGSTON DEPT OF MECHANICAL ENGINEERING AND.. M H SADD ET AL. 1/1

UNCLASSIFIED JUL 84 ARO-18477.4-GS DAAG29-82-K-0012 F/G 20/14 NL

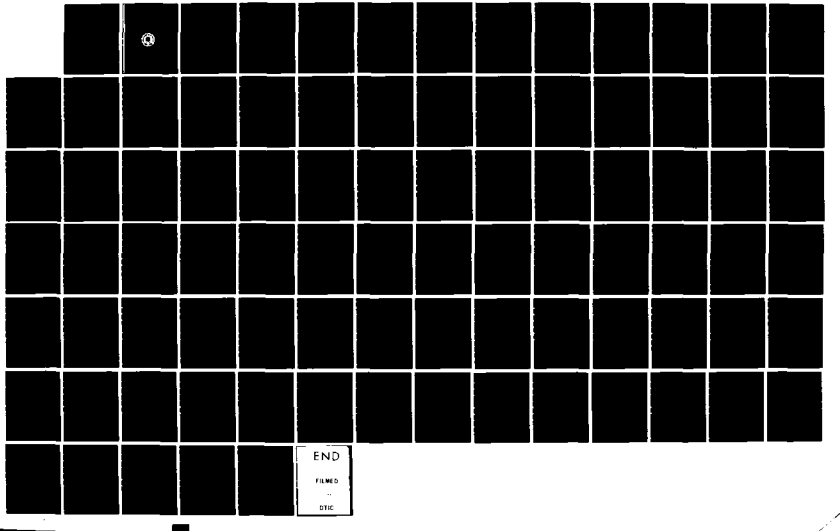

END

FILMED

DTIC

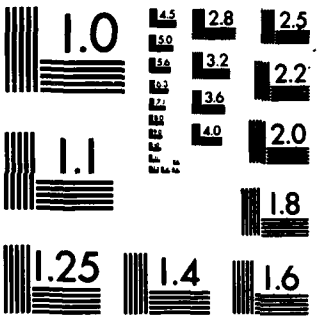

MICROCOPY RESOLUTION TEST CHART
NATIONAL BUREAU OF STANDARDS-1963-A

ARO 18477.4-GS

Final Report

Analysis of In-Plane and Out-of-Plane Ground Motions Using the Boundary Element Method

by

Martin H. Sadd
John M. Rice

Prepared for

The U. S. Army Research Office
Under Contract No. DAAG29-82-K-0012

Department of

Mechanical Engineering and Applied Mechanics
University of Rhode Island
Kingston, RI, 02881

July 1984

Analysis of In-Plane and Out-of-Plane Ground Motions Using the Boundary Element Method

FINAL REPORT

by

Martin H. Sadd
John M. Rice

July 1984

U.S. ARMY RESEARCH OFFICE

Contract No. DAAG29-82-K-0012

University of Rhode Island
Department of Mechanical Engineering & Applied Mechanics
Kingston, RI

MASTER COPY - FOR REPRODUCTION PURPOSES

REPORT DOCUMENTATION PAGE

READ INSTRUCTIONS BEFORE COMPLETING FORM

1. REPORT NUMBER: ARO 18477.4-GS	2. GOVT ACCESSION NO.: AD-A146 229 N/A
3. RECIPIENT'S CATALOG NUMBER: N/A	
4. TITLE (and Subtitle): Analysis of In-Plane and Out-of-Plane Ground Motions Using the Boundary Element Method	5. TYPE OF REPORT & PERIOD COVERED: Final Report 1/1/82 - 5/31/84
	6. PERFORMING ORG. REPORT NUMBER
7. AUTHOR(s): Martin H. Sadd, John M. Rice	8. CONTRACT OR GRANT NUMBER(s): DAAG29-82-K-0012
9. PERFORMING ORGANIZATION NAME AND ADDRESS: University of Rhode Island, Department of Mechanical Engineering & Appl.Mechanics, Kingston, RI 02881	10. PROGRAM ELEMENT, PROJECT, TASK AREA & WORK UNIT NUMBERS
11. CONTROLLING OFFICE NAME AND ADDRESS: U. S. Army Research Office, Post Office Box 12211, Research Triangle Park, NC 27709	12. REPORT DATE: July 1984
	13. NUMBER OF PAGES: 79
14. MONITORING AGENCY NAME & ADDRESS(if different from Controlling Office)	15. SECURITY CLASS. (of this report): Unclassified
	15a. DECLASSIFICATION/DOWNGRADING SCHEDULE

16. DISTRIBUTION STATEMENT (of this Report)

Approved for public release; distribution unlimited.

17. DISTRIBUTION STATEMENT (of the abstract entered in Block 20, if different from Report)

NA

18. SUPPLEMENTARY NOTES

The view, opinions, and/or findings contained in this report are those of the author(s) and should not be construed as an official Department of the Army position, policy, or decision, unless so designated by other documentation.

19. KEY WORDS (Continue on reverse side if necessary and identify by block number)

Ground Motion, Wave Propagation, Boundary Element Method, Geomechanics, Elastodynamics

20. ABSTRACT (Continue on reverse side if necessary and identify by block number)

A completed research program is presented which has developed new computational methods to study geomechanics ground motions excited by subsurface sources. Both in-plane (plane strain) and out-of-plane (anti-plane strain) motions are investigated by employing a direct boundary element method within the framework of linear dynamic elasticity theory. The constructed boundary element method uses a time-dependent, half-space Green's function; thereby, eliminating the need to discretize the free surface, allowing the causality principle to reduce the number of required computations, and permitting an

DD FORM 1 JAN 73 1473 EDITION OF 1 NOV 65 IS OBSOLETE

explicit time stepping scheme to be developed. The method is applicable for transient waves of general form propagating in an elastic half-space with arbitrary buried cavities. Numerical examples of both in-plane and out-of-plane problems are presented.

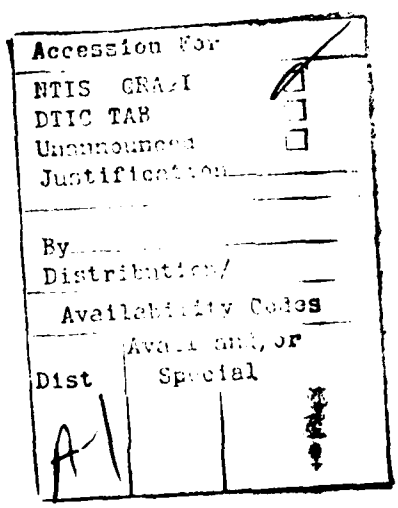

TABLE OF CONTENTS

TABLE OF CONTENTS

(Continued)

LIST OF FIGURES

LIST OF FIGURES

(Continued)

I. INTRODUCTION

The completed research herein described is concerned with theoretical/computational modeling of mechanical signal transmission through soil media from subsurface sources. The propagation of such signals plays a central role in detecting or sensing dynamic subsurface events. A source below the surface will transmit stress waves in all directions. These waves will interact with the surrounding surface and any buried objects, and will produce a dynamic wave motion field. By incorporating a proper measurement field array, data may be gathered on the field to predict the nature of the source. Mathematical predictions of both surface and subsurface wave motion patterns would act as a guide for optimal sensor arrays and logic in order to determine these source signatures.

The propagation and scattering of elastic waves by cavities and cracks has been the subject of numerous investigations during the past several years. Early studies have dealt with the cases of cavities in infinite media, while more recent work, Sanchez-Sesma [46], Stone et. al. [50], Mendelsohn et. al. [34], Achenbach and Brind [3], Datta and El-Akily [18], Shah et. al. [47], and Abduljabbar et. al. [1], has been directed at scattering problems in semi-infinite domains. For semi-infinite regions (near field soil modeling) the presence of the free surface influences the scattering wave field, and this phenomena becomes important in a wide variety of dynamic geomechanics problems including seismology, blast loading, sensing, mineral exploration, etc.

Wave propagation problems quickly become difficult to analyze as the boundary geometry becomes complex. At this point one usually turns to some numerical method that will approximate the solution for this geometry. The methods of finite differences and finite elements have

become very popular in wave propagation studies. These methods are sometimes called domain methods because the entire field of the physical problem is discretized into small areas or cells. For example, Reynolds [42] and Kelley et. al. [25] have developed finite difference codes for two-dimensional wave propagation. Other finite difference and finite element work can be found in Alder [5] which reviews a broad class of problems. When modeling wave propagation, these domain methods have limitations in properly representing the boundaries of the body under study and have trouble if the domains are large or infinite. Bouchon and Aki in a series of articles [8,9,10] presented an alternate numerical approach called the discrete wave number representation method. Ray methods have also been applied for approximate answers to such problems see for example Achenbach, Gautsen, and McMaken [4].

After a review of these previous techniques one finds several difficulties associated with each method. Consequently a somewhat new approach was taken in which a numerical technique was developed based on an integral formulation of the elastodynamic equations. Integral formulations in elasticity theory have a long history dating back to the 19th century. However, although such formulations have been known for quite some time, their application for developing numerical algorithms for use in problem solutions is relatively new. Recently many investigators have been employing integral formulations with numerical methods (including finite element concepts) to solve a broad class of both static and dynamic elasticity problems. These methods have become known as the Boundary Integral Equation Method (BIE or BIEM) or the Boundary Element Method (BEM). The recent texts by Brebbia [11], Brebbia and Walker [12] and Banerjee and Butterfield [6] provide general background for these methods as they are applied to a large variety of

engineering science problems.

With regard to elastodynamic problems, Cruse and Rizzo [17] and Cruse [16] developed a BEM approach in conjunction with Laplace transformation. Niwa et. al. [39,40] and Kobayashi and Nishimura [27] used BEM methods for the steady state solution and then reconstructed the transient response by Fourier synthesis. Shaw [48] also discusses the steady state solution using a Fourier transform. Cole, Kossloff, and Minster [15], Mansur and Brebbia [32,33], and Misljenovic [37,38] have developed a time-dependent formulation which eliminates the need for Laplace transformation and/or Fourier synthesis. Manolis [31] has recently compared these three BEM methods on a scattering proble .. an infinite medium, and found that all three methods gave good resul'

Using the BEM with transform methods, after one obtains a so.t' , in the Laplace or Fourier domain, one must invert it to solve for the time domain solution. Transform methods also require the solution of a full matrix and do not take advantage of the causal properties that the time-dependent Green's function possesses. The direct BEM time domain approach has economical advantages because of this, as it permits an explicit stepping scheme which will result in a banded solution matrix.

Fundamental to the application of the Boundary Element Method is a Green's function (fundamental solution) to the governing equations. The ease and efficiency of the method is connected quite closely with the nature of the Green's function that is employed. All of the previously mentioned studies have used the Green's function for an infinite domain, thus requiring all boundaries to be discretized. Kobayashi and Nishimura [28] constructed a half-space Green's function for the steady state elastodynamic case, but did not utilize it. It has been demonstrated by Telles and Brebbia [51] for the static elasticity case, that by using a

half-space Green's function, considerable simplification is gained for half-space geomechanics problems. A major goal of this research was to extend Telles' and Brebbia's idea to dynamic wave propagation phenomena. This has involved the development of an easily computable Green's function for a half-space domain, and its implimentation into a general purpose, two-dimensional boundary element numerical code. The created numerical methods are designed for half-space problems involving propagation and scattering of near field transient elastic waves. Solution methods for both anti-plane strain (out-of-plane motions) and plane strain (in-plane motions) are developed.

II. BASIC ELASTODYNAMIC THEORY

2.1 Basic Equations of Elastodynamics

The basic variables in dynamic elasticity theory are the stresses σ_{ij}, the strains e_{ij} and the displacements u_i. The general field equations relate these variables to one another and provide the basis of the theory (see Achenbach [2], Graff [23] or Ewing et.al. [21]). From kinematics the strain-displacement relations are given by

$$e_{ij} = \frac{1}{2}\,(u_{i,j} + u_{j,i}) \tag{2.1}$$

Due to the conservation of linear momentum we can express Newton's law as the equation of motion for a continum,

$$\sigma_{ij,j} + \rho f_i = \rho \ddot{u}_i, \tag{2.2}$$

where f_i is the body force density and ρ is the mass density. The constitutive law for a linear elastic isotropic material is given by

Hooke's law as

$$\sigma_{ij} = \lambda e_{kk}\delta_{ij} + 2\mu e_{ij}, \tag{2.3}$$

where λ and μ are elastic constants.

Combining equations (2.1), (2.2), (2.3), we can eliminate the stresses and strains to get Navier's equation of motion in terms of displacement

$$\mu u_{i,kk} + (\lambda+\mu)u_{k,ki} + \rho f_i = \rho \ddot{u}_i \tag{2.4}$$

There are normally three types of boundary conditions prescribed on the boundary surface of a body.

1) A distribution of surface forces or tractions $\underline{t}$, on the surface of the body, where

$$t_i = \sigma_{ij} n_j$$

with n_i being the unit normal vector.

2) A distribution of displacements $\underline{u}$, on the surface of the body.

3) A distribution of surface forces on a portion of the boundary surface and displacements on the remaining portion.

These along with initial conditions on the displacement and velocity provide the necessary conditions which when coupled with the governing equations produce a unique solution. The proof of this can be found in Wheeler and Sternberg [52] or Sokolnikoff [49].

2.2 Dilatation and Shear Wave Motion

If we take the divergence of the equation of motion (2.4) without body forces, we get an equation associated with irrotational wave motion, i.e.

$$u_{i,ikk} = \frac{1}{c_1^2} \ddot{u}_{i,i}, \tag{2.5}$$

where $u_{i,i}$ is the dilatation (volume changing motion) and $c_1 = [(\lambda + 2\mu)/\rho]^{1/2}$. This irrotational or dilatational wave motion is associated with what is commonly called a P-wave which propagates with velocity c_1.

Taking the curl of equation (2.4) without body forces, we get an equation associted with rotational wave motion.

$$u_{i,kk} = \frac{1}{c_2^2} \ddot{u}_i, \tag{2.6}$$

where $c_2 = (\mu/\rho)^{1/2}$. This rotational (volume preserving motion) or shear wave motion is commonly refered to as an S-wave and propagates with velocity c_2.

In an infinite medium an internal input disturbance will in general produce both dilatation and shear motions. Thus a general disturbance will propagate to remote points as two different wave motions.

2.3 Helmholtz Decomposition Theorem

The Helmholtz Decomposition Theorem states that a vector field $\underline{u}$ that is sufficiently smooth i.e. satisfies certain continuity requirements, may be written as the sum of the gradient of a scalar potential function plus the curl of a vector function, i.e.

$$\underline{u} = \underline{\nabla}\phi + \underline{\nabla} \times \underline{\psi}, \tag{2.7}$$

with the condition

$$\underline{\nabla} \cdot \underline{\psi} = 0 .$$

Using this form of $\underline{u}$ as a displacement vector and substituting into equation (2.4) without body forces, yields

$$\nabla^2\phi = \frac{1}{c_1^2}\ddot{\phi} \quad , \quad \nabla^2\underline{\psi} = \frac{1}{c_2^2}\ddot{\underline{\psi}} . \tag{2.8}$$

Note that the displacement potential ϕ is associated with the dilatation wave and $\underline{\psi}$ is associated with the shear wave.

This decomposition is useful for many elastodynamic problems, since the complex equation of motion (2.4) is reduced to two simple uncoupled wave equations. It should be mentioned here however, that the two potentials are coupled through the boundary conditions since the displacements and stresses depend on both ϕ and Ψ .

2.4 Two Dimensional Elastodynamics

Plane Strain

For bodies that are very long in one direction and loaded in a plane perpendicular to this direction we can make certain approximations that will simplify the general equation of motion (2.4). This case is known as plane strain and the displacements are of the form

$$\begin{aligned} u &= u(x_1, x_2, t) \\ v &= v(x_1, x_2, t) \\ w &= 0 \end{aligned} \tag{2.9}$$

Note that this corresponds to in-plane motions.

The non-zero strain components are given by

$$e_x = \frac{\partial u}{\partial x_1}$$

$$e_y = \frac{\partial v}{\partial x_2} \qquad (2.10)$$

$$e_{xy} = \frac{1}{2}\left(\frac{\partial u}{\partial x_2} + \frac{\partial v}{\partial x_1}\right)$$

and the non-zero stress components are

$$\begin{aligned} \sigma_x &= \lambda(e_x+e_y)+2\mu e_x \\ \sigma_y &= \lambda(e_x+e_y)+2\mu e_y \\ \sigma_z &= \lambda(e_x+e_y) \\ \tau_{xy} &= 2\mu e_{xy}. \end{aligned} \qquad (2.11)$$

The equation of motion in terms of displacement becomes

$$\mu \nabla^2 \underline{u}+(\lambda+\mu)\underline{\nabla}(\underline{\nabla}\cdot\underline{u})+\rho\underline{f} = \rho\ddot{\underline{u}} \qquad (2.12)$$

where

$$\underline{\nabla} = \underline{i}\,\frac{\partial}{\partial x_1} + \underline{j}\,\frac{\partial}{\partial x_2}\,.$$

Waves associated with this equation will either be dilatation waves (P-waves) or vertically polarized shear waves (SV-waves).

Plane Stress

For bodies that are very thin in one direction and loaded in a plane perpendicular to this direction we can again make certain approximations that will simplify the basic equation of motion. This case is refered to as plane stress and the stress components are taken to be

$$\begin{aligned} \sigma_x &= \sigma_x(x_1,x_2,t) \\ \sigma_y &= \sigma_y(x_1,x_2,t) \\ \tau_{xy} &= \tau_{xy}(x_1,x_2,t) \\ \sigma_z &= \tau_{xz} = \tau_{yz} = 0 \end{aligned} \tag{2.13}$$

The non-zero strain components will then be

$$\begin{aligned} e_x &= (\sigma_x+\nu\sigma_y)/E \\ e_y &= (\sigma_y+\nu\sigma_x)/E \\ e_z &= (\sigma_x+\sigma_y)/E \\ e_{xy} &= \tau_{xy}/2\mu, \end{aligned} \tag{2.14}$$

while the equation of motion in terms of displacement reduces to

$$\mu\nabla^2\underline{u} + \frac{E}{2(1-\nu)}\,\underline{\nabla}(\underline{\nabla}\cdot\underline{u})+\rho\underline{f} = \rho\ddot{\underline{u}} \tag{2.15}$$

where E and ν are elastic constants.

Anti-Plane Strain

Bodies that are very long in one direction and loaded parallel to that direction can again be modeled by making certain approximations that will simplify the basic three dimensional equations of motion. This case is normally referred to as anti-plane strain and the displacements are of the form

$$\begin{aligned} u &= 0 \\ v &= 0 \\ w &= w(x_1,x_2,t). \end{aligned} \tag{2.16}$$

This case corresponds to out-of-plane motions.

The non-zero strain components follow from (2.1) to be

$$e_{yz} = \frac{\partial w}{\partial x_2} \qquad (2.17)$$
$$e_{xz} = \frac{\partial w}{\partial x_1}$$

and the non-zero stress components, from Hook's law, are

$$\sigma_{zx} = 2\mu e_{zx} \qquad (2.18)$$
$$\sigma_{zy} = 2\mu e_{zy}$$

For this case the equation of motion in terms of displacement reduces to

$$\mu\nabla^2 w + \rho f = \rho\ddot{w} \qquad (2.19)$$

Waves associated with this anti-plane case will be horizontally polarized shear waves (SH-waves).

2.5 Ray Theory

The purpose of this section is to review how plane P-,SV-, and SH-waves reflect from stress free plane surfaces. The geometrical nature of these incident and reflecting waves is sometimes called ray theory. For plane strain, the free surface will produce a coupling (mode conversion) between the SV-wave and the P-wave i.e., the incident P-wave or SV-wave will produce both reflected P-waves and SV-waves.

All cases are related through Figure 2.1 which illustrates the basic ray patterns. The incident wave (either P or S) has an incident angle θ_0, measured from the surface normal. The reflected P-wave has angle $,\theta_1$, while the reflected S-wave has angle θ_2.

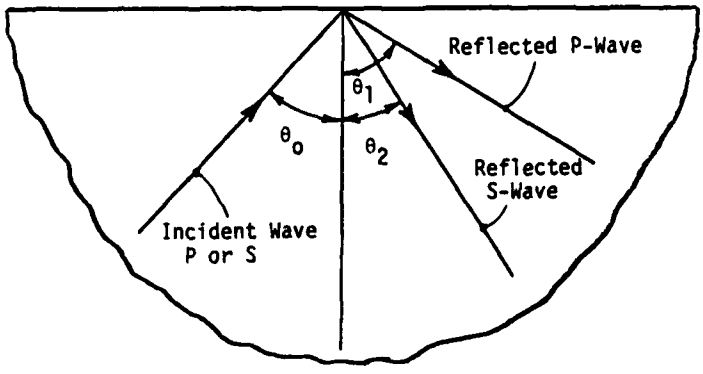

Fig. 1 Ray Theory

For the anti-plane strain case, there will be no mode conversion and hence only a single reflected SH-wave will be present with the incident and reflected angles being equal, i.e.

$$\theta_2 = \theta_o \tag{2.20}$$

For plane strain we have two possible types of incident waves the P-wave and the SV-wave. In both cases there is in general a mode conversion where either the P-wave or SV-wave will upon reflection become part P-wave and part SV-wave; see Figure 2.1.

For an incident P-wave,

$$\theta_1 = \theta_o \tag{2.21}$$

$$c_2 \sin \theta_o = c_1 \sin \theta_2, \tag{2.22}$$

while for an incident SV-wave

$$\theta_2 = \theta_o \tag{2.23}$$

$$c_2 \sin\theta_1 = c_1 \sin\theta_o \tag{2.24}$$

Note equation (2.23) is real-valued only if $\theta_o \leq \sin^{-1}(c_2/c_1)$ otherwise there is a mode conversion of the SV-wave to a surface wave.

The previous equations provide information necessary to compute directly the angles and ray path distances of reflected and incident plane waves, except in the case of the reflected SV-wave from an incident P-wave and the reflected P-wave from an incident SV-wave. To find the ray path distances for these two exceptions we must turn to numerical techniques.

Figure 2.2 illustrates a typical source/receiver pair in plane strain, where the source is at (0,h) and the receiver is at (x,y). Consider a ray path SPR as shown, depicting an incident P-wave traveling a distance c, and a reflected SV-wave traveling a distance d. With x = a+b, these ray paths c and d can be found from two simultaneous nonlinear equations

$$h^2 + \left[x - \frac{Kxd}{c+Kd}\right]^2 = c^2 \tag{2.25}$$

$$y^2 + \left[\frac{Kxd}{c+Kd}\right]^2 = d^2,$$

where, $K = c_2/c_1$. These equations can be solved by employing the Newton method see Rice [45], Ketter and Sherwood [26] and Berezin and Zidkov [7].

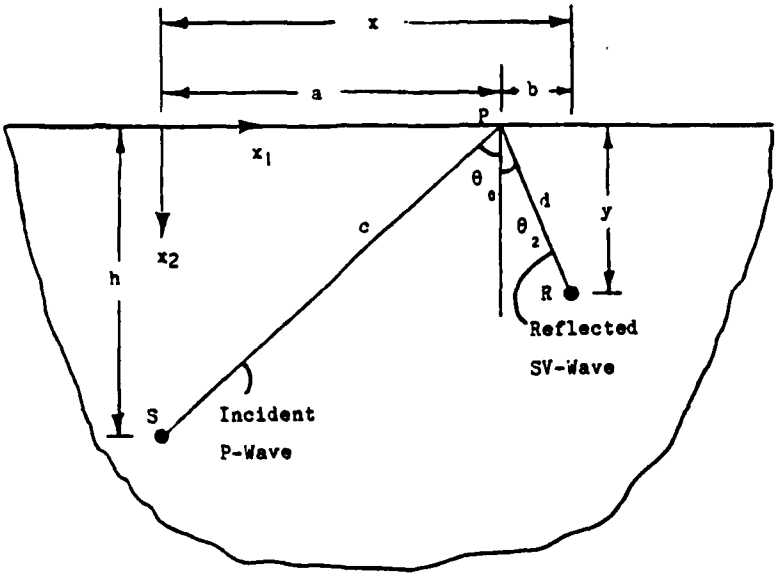

Fig. 2.2 Geometry of Incident P-Wave and Reflected SV-Wave

Figure 2.3 illustrates another typical source/receiver pair in plane strain, where the SV-source is at (0,h) and the receiver is at (x,y). Consider now a ray path SPR as shown, where an incident SV-wave travels a distance c, and a reflected P-wave travels a distance d. With x = a+b, these ray paths can be found from two simultaneous equations

$$h^2+[x-\frac{xd}{Kc+d}]^2 = c^2$$
$$y^2+[\frac{xd}{Kc+d}]^2 = d^2 \qquad (2.26)$$

These equations can again be solved by employing the Newton method.

Figure 2.4 illustrates the case of waves with equal angles of incidence and reflection. This occurs for the SH, P-P and SV-SV cases. Again the source is at (0,h) and the receiver is at (x,y), and c and d are the ray paths of incidence and reflection. For this case

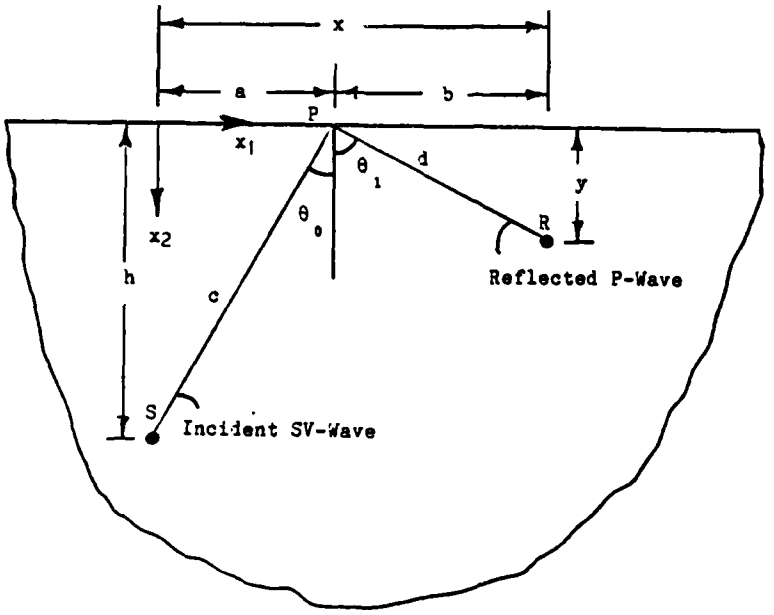

Fig. 2.3 Geometry of Incident SV-Wave and Reflected P-Wave

$$c = h\left[1 + \left(\frac{x}{h+y}\right)^2\right]^{1/2}$$
$$d = y\left[1 + \left(\frac{x}{h+y}\right)^2\right]^{1/2}. \qquad (2.27)$$

2.6 Integral Representations

For the general elastodynamic problem, we may obtain an integral equation from the dynamic reciprocal theorem which is the direct extension of Betti's reciprocal theorem in elastostatics. The theorem states that two unrelated elastodynamic states consisting of body forces, surface tractions and displacements, initial conditions and velocities, such as $\{f_i, t_i, u_i, u_i', v_i'\}$ and $\{\tilde{f}_i, \tilde{t}_i, \tilde{u}_i, \tilde{u}_i', \tilde{v}_i'\}$ which exist on the same body S

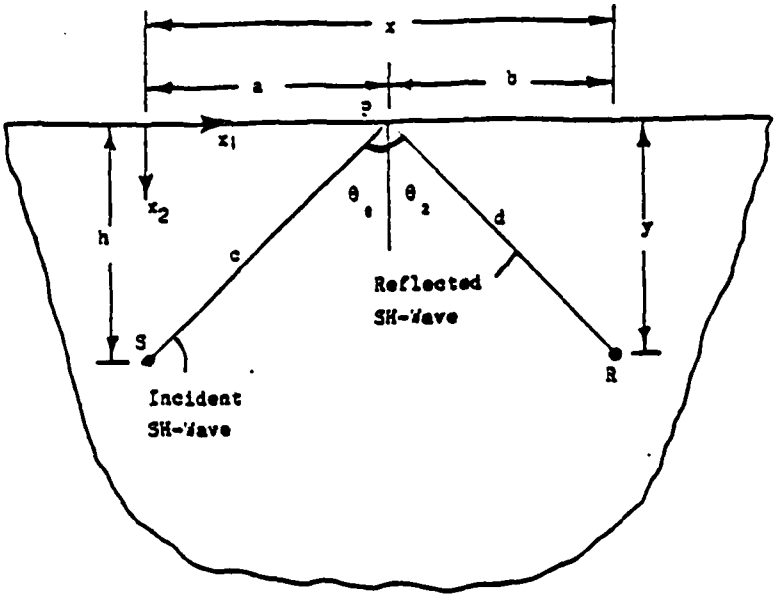

Fig. 2.4 Geometry of Incident SH-Wave and Reflected SH-Wave

bounded by a surface ∂S for $t > 0$, are related by

$$\int_{\partial S} [(t_i * \tilde{u}_i)(x,t)]dS + \int_S \rho[(f_i * \tilde{u}_i)(x,t) + v_i'(x)\tilde{u}_i(x,t) + u_i'(x)\frac{\partial \tilde{u}_i}{\partial t}(x,t)]dv = \int_{\partial S}[t_i * u_i)(x,t)]dS + \int_S \rho[(\tilde{f}_i * u_i)(x,t) + \tilde{v}_i'(x)u_i(x,t) + \tilde{u}_i'(x)\frac{\partial u_i(x,t)}{\partial t}]dv \quad (2.28)$$

where * means the convolution integral defined by

$$(f*g)(x,t) = \begin{cases} \int_0^t f(x,t-\tau)g(x,\tau)d\tau, & t \geq 0 \\ 0, & t < 0 . \end{cases} \quad (2.29)$$

If we choose one of the elastodynamic states say $(f_i, t_i, u_i, u_i', v_i')$ to be that of the physical problem and let the other state $(\tilde{f}_i, \tilde{t}_i, \tilde{u}_i, \tilde{u}_i', \tilde{v}_i')$ be

that generated by a unit concentrated body force in the same body, we obtain the integral expression

$$c\underline{u}(\underline{r}_o,t_o)=\int_0^\infty\int_{\partial S}\{\underline{\underline{G}}\underline{\tau}(\underline{r},t)-\underline{u}(\underline{r},t)\underline{\underline{K}}\cdot n\}dS(\underline{r})dt, \tag{2.30}$$

where we have neglected the body force f_i and taken zero initial conditions. The coefficient c is given by

$$c=\begin{cases} 1/2, & r \in \text{smooth boundary } \partial S \\ 1, & r \in \text{interior of } \partial S \\ 0, & r \in \text{exterior of } \partial S \end{cases} \tag{2.31}$$

$\underline{\underline{G}}=\underline{\underline{G}}(r,t;r_o,t_o)$ is the displacement Green's function, $\underline{\underline{K}}$ is the stress field associated with $\underline{\underline{G}}$, $\underline{\tau}$ and $\underline{u}$ are the surface tractions and displacements on the boundary ∂S, $\underline{r}_o$ and $\underline{t}_o$ are the space and time positions of the source (associated with the Green's function), $\underline{r}$ and $\underline{t}$ are the space and time positions of the receiver, and $\underline{n}$ is the unit normal vector to the surface. Subscripts "o" refer to source quantities. Details on the Green's functions will be provided later in the report.

For the anti-plane strain case, the integral relation may be written as

$$cw(\underline{r},t) = \int_0^\infty\int_{\partial S}\{G\tau(\underline{r}_o,t_o)-w(\underline{r}_o,t_o)\underline{K}\cdot\underline{n}\}dS(\underline{r}_o)dt_o, \tag{2.32}$$

where we now have a scalar equation.

III THE BOUNDARY ELEMENT METHOD

3.1 Principal Advantages

Recently a new numerical method has been developed called the Boundary Integral Equation Method. The basic method when combined with finite element discretization concepts is commonly refered to as the Boundary Element Method. The method is applicable to a wide variety of field problems in engineering science and has some advantages over the finite element and finite difference methods in several situations.

The principal advantages of the BEM method lie primarily in the reduction of the number of spatial dimensions of the problem by one, and by formulating the problem directly in terms of the boundary values. Since discretization is carried out only on the boundary of the body under study, the number of unknowns in the numerical problem is reduced, and the need of creating space-filling, three-dimensional grids is eliminated. For many cases, problems involving infinite domains can be handled in a very direct and simple manner using appropriate Green's functions. For infinite or semi-infinite problems there will be considerably fewer elements and thus a smaller system of equations need be solved.

Another advantage over domain methods has to do with the solution variables inside the body. These variables in domain methods will often show unrealistic jumps in values between nodal points and will not vary continuously. In the BEM method these variables will vary continuously in the body as the only approximations of geometry occur on the boundary. In many engineering problems the important part of the solution will be on the boundary or at a few selective points in the interior. With domain methods the solution is found at all nodal values, while in the BEM method the solution is found for boundary nodes and only

those interior points selected by the user. As in the finite difference and finite element methods, the problem is reduced to a system of simultaneous equations to be solved. While in the domain methods the system coefficient matrix is usually banded, using the BEM this matrix can be fully populated.

3.2 Method Development

The development of the BEM method for a general problem is described in the flow chart in Figure 3.1. The method is started with the use of

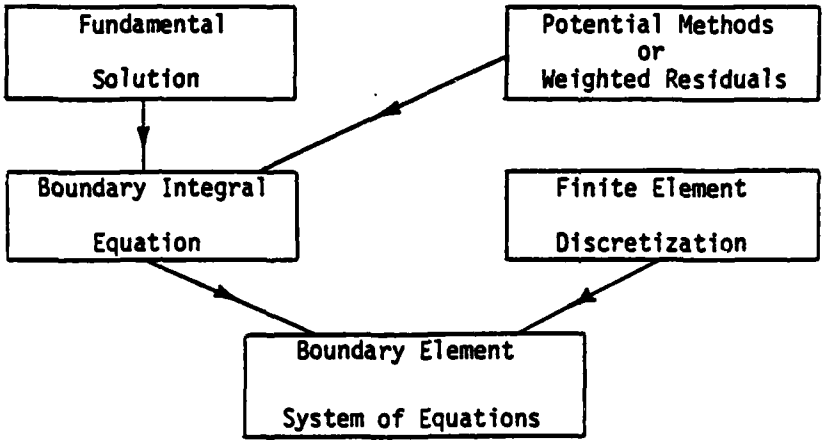

Fig. 3.1 Flow Chart of Boundary Element Method

potential theory or weighted residual methods which when combined with a Green's function, form the boundary integral equation. The use of an efficient Green's funciton is central to the method. There are multiple choices for a Green's function, all of which will satisfy the governing equation for the problem, but will vary according to the boundary conditions on the body. Again refering to Figure 3.1, the boundary

integral equation is then discretized using established finite element techniques to form a system of simultaneous linear algebraic equations. The solution to these equations will yield the unknown boundary values of the problem. These boundary values can in turn be used to find the solution at any interior points.

The basis for an integral equation formulation in elastodynamics was first developed by Kupradze [29], de Hoop [19] and Wheeler and Sternberg [52], while Eringen and Suhubi [20] provide a concise review of this classical work. The integral equation formulation is the dynamic extension of Betti's reciprocal theorem which relates two different dynamic states for a given elastic body, see equation (2.28). An apparent choice for one of the two elastodynamic states is the desired solution to the problem, while the other state is normally chosen to be an appropriate Green's function that satisfies the governing equations of motion for the problem under study. Using these choices, the dynamic equivalent to Somigliana's identity can be derived, e.g. equation (2.30), and through a limiting process a boundary integral equation is developed which forms the basis of the BEM method. This process was outlined in section 2.6, and developes what is called a direct BEM approach, see Mendelson [35].

3.3 Half-Space Green's Function for Geomechanics Problems

If one were to model a typical geomechanics problem of a buried hole using a finite element technique, a typical mesh might look like Figure 3.2. As can be seen in this figure there are problems in determining how far out to run the mesh and what boundary conditions to use on the outer elements. The BEM method will eliminate the need for a space filling

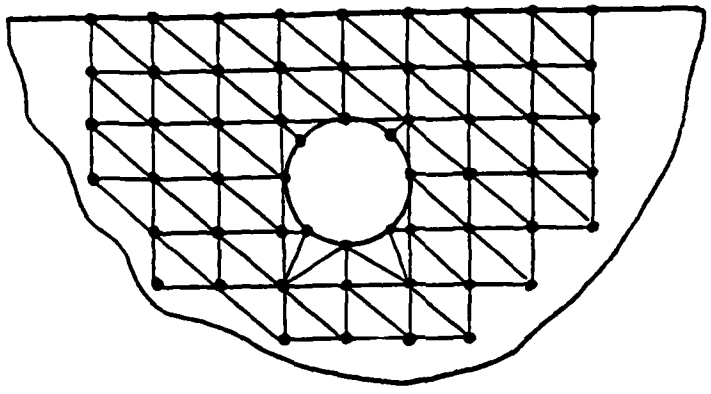

Fig. 3.2 Finite Element Interior Discretization for a Buried Hole

mesh as can be seen in Figure 3.3a where this discretization is a result of using the BEM with an infinite space Green's function. Again however, problems appear as to how far out to run the boundary mesh and what

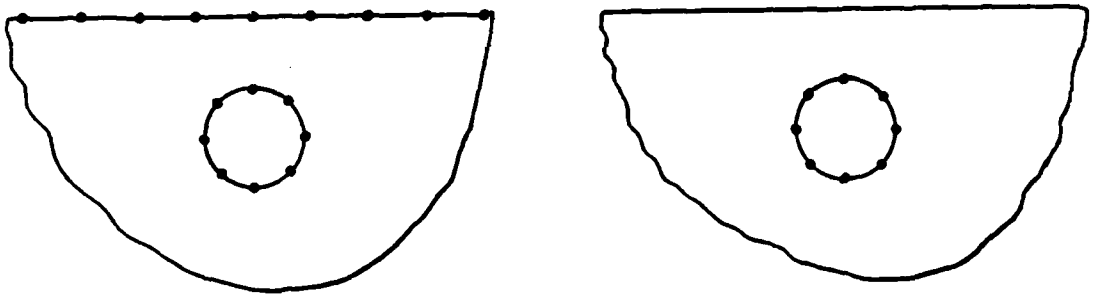

a. Infinite Space Green's Function b. Half-Space Green's Function

Fig. 3.3 BEM Discretization for Buried Hole

boundary conditions to use on the outer elements. These problems can be eliminated with the use of a half-space Green's function as shown in Figure 3.3b, where now there is no need to discretize the free surface since that boundary condition is automatically satisfied by the half-space Green's function. This example brings out the importance of the choice of the Green's function, and illustrates the usefulness of a

half-space form for geomechanics problems. The employment of such a half-space Green's function was a major part of this research program.

IV GREEN'S FUNCTIONS

4.1 Introduction

The Green's function is the singular solution of a differential equation subjected to an impulsive source. In the case of elastodynamics the governing equation is Navier's equation of motion (2.4), and the source is taken as a concentrated impulsive body force loading. The Green's function may be developed for regions of infinite extent or for regions of finite size with particular boundary conditions. As demonstrated in section 3.3, the development of a Green's function for a semi-infinite domain is most desired for geomechanics applications.

Elastodynamic problems for half-spaces subject to impulsive buried point loads or other sources have been studied for quite some time, see e.g. Lamb [30], Hudson [24], Eringen and Suhubi [20], Payton [41], and Garvin [22]. These types of problems are directly related to fundamental singular solutions (i.e. Green's functions) for the half-space geometry. For the anti-plane strain case, such solutions can be found in Cole et.al. [15], Achenbach [2], Rice and Sadd [44], and Hudson [24]. Singular force solutions for the plane strain case are complex and are obtained by integral transform methods with the inversion being accomplished by employing some version of the Cagniard [13] technique. Because of mathematical difficulties, most of these solutions are formally carried out only for surface points or other special points in the medium.

With a fundamental Green's function for a half-space geometry, the BIE method can be used quite effectively to handle many dynamic geomechanics problems, see for example Rice and Sadd [43,44]. However in order to use a fundamental solution in this way, it must be computable at all points in the region. Hence the development of easily computable Green's functions is very important in constructing efficient numerical BEM codes for wave propagation.

We present here the development of an elastodynamic Green's function for a two-dimensional, isotropic half-space. For anti-plane strain, we consider the buried singular impulsive line load and construct a half-space Green's function from the infinite space Green's function by the method of images. For plane strain, we address the buried singular impulsive line load as formulated by Hudson [24]. Starting with the formal solution, a numerical root finding scheme is employed to compute terms which normally present problems for points below the free surface.

4.2 Anti-Plane Strain Green's Function

Rewriting the anti-plane strain equation of motion equation (2.19)

$$\mu\nabla^2 w+\rho f = \rho\ddot{w}, \tag{4.1}$$

if we let ρf be a concentrated impulsive out of plane line load at r_o and t_o, w will now become the anti-plane strain Green's function G. For this case equation (4.1) becomes

$$\mu\nabla^2 G-\rho\ddot{G} = -\delta(t-t_o)\delta(\underline{r}-\underline{r}_o). \tag{4.2}$$

For the infinite space domain, G is given by

$$G(\underline{r},t;\underline{r}_o,t_o) = \frac{1}{2\pi\mu} \frac{H(t-t_o-R/c_2)}{[(t-t_o)^2-R^2/c_2{}^2]^{1/2}} \tag{4.3}$$

where $R = |\underline{r}_o - \underline{r}|$ and H is the Heaviside function.

The stress field associated with this Green's function is computed through Hooke's law and is given by

$$\underline{K}(\underline{r},t;\underline{r}_o,t) = \frac{R}{2\pi c_2{}^2} \frac{H(t-t_o-R/c_2)}{[(t-t_o)^2-R^2/c_2{}^2]^{3/2}} \frac{\partial R}{\partial \underline{n}} . \tag{4.4}$$

For the anti-plane strain half-space problem, the method of images can be used to construct a half-space Green's function from the infinite space Green's function through the superposition of a virtual infinite space function of equal amplitude with an image source point relative to the free surface as shown in Figure 4.1. The associated stress field can

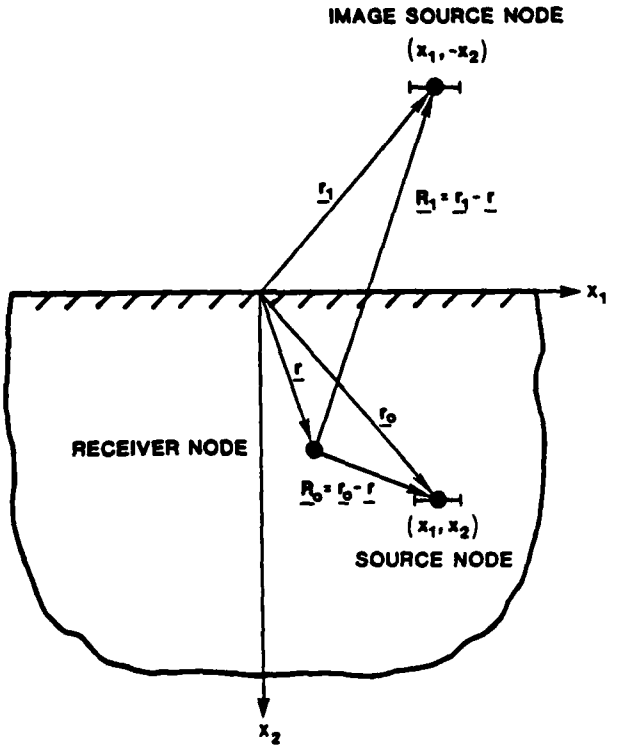

Fig. 4.1 Geometry of Source and Image for the Construction of a Half-Space Green's Function

be derived as in (4.4). The results are

$$G=G_0+G_1=\frac{1}{2\pi\mu}\left\{\frac{H(t-t_0-R_0/c_2)}{[(t-t_0)^2-R_0^2/c_2^2]^{1/2}}+\frac{H(t-t_0-R_1/c_2)}{[(t-t_0)^2-R_1^2/c_2^2]^{1/2}}\right\} \quad (4.5)$$

$$\underline{K}=\underline{K}_0+\underline{K}_1=\frac{1}{2\pi c_2^2}\left\{\frac{R_0H(t-t_0-R_0/c_2)}{[(t-t_0)^2-R_0^2/c_2^2]^{3/2}}\frac{\partial R_0}{\partial \underline{n}}+\frac{R_1H(t-t_0-R_1/c_2)}{[(t-t_0)^2-R_1^2/c_2^2]^{3/2}}\frac{\partial R_1}{\partial \underline{n}}\right\} \quad (4.6)$$

where the position vectors R_0 and R_1 are defined in Figure 4.1. This simple superposition produces a stress free surface at $x_2 = 0$ as required. The advantage of using the half-space form in the BEM method is that the boundary of the free surface will not have to be discretized, thus simplifying the problem.

4.3 Plane Strain Green's Function

The plane strain equations of motion (2.12) in indicial notation are

$$\mu u_{k,ii} + (\lambda+\mu)u_{i,ik} + \rho f_k = \rho \ddot{u}_k \quad (4.7)$$

If we let ρf_k be a concentrated in-plane line load located at $x_1 = 0$, $x_2=h$ and $u_i=G_{ij}e_j$ where e_j is a unit vector in the x_1,x_2 plane, then G_{ij} is interpreted as the two-dimensional Green's function. This Green's function G_{ij} evaluates the displacement field u_i due to a concentrated unit force in the e_j direction. Equation (4.7) then becomes

$$\mu G_{ij,kk} + (\lambda+\mu)G_{kj,ik} - \rho G_{ij} = \delta(t)\delta(x_1)\delta(x_2-h)\delta_{ij} \quad (4.8)$$

Introducing displacement potentials and using Fourier transformation methods with the Cagniard [13] inversion technique, Hudson [24] develops a solution to (4.8) for a stress free surface with zero initial conditions. The reflected portion of the wave field is found to be

$$G_{ij}^{R} = \frac{1}{2\pi\rho}\,[H(t-r''/c_1)U_{ij}^{PP} + H(t-t_{SP})U_{ij}^{SP} + H(t-t_{PS})U_{ij}^{PS} + H(t-r''/c_2)U_{ij}^{SS} + H(t-t_{SPS})H(r''/c_2-t)U_{ij}^{SPS}], \tag{4.9}$$

where t is the actual time, r" is the distance between the image source and receiver, and r' is the distance between the source and receiver.

U_{ij}^{PP} is the displacement tensor for an incident P-wave producing a reflected P-wave,

$$U_{ij}^{PP} = \mathrm{Re}\left\{ \begin{bmatrix} s^2/\eta_\alpha & -is \\ is & \eta_\alpha \end{bmatrix} \frac{S(s)}{R(s)} \frac{ds}{dt} \right\}. \tag{4.10}$$

U_{ij}^{PS} is the displacement tensor for an incident P-wave producing a reflected S-wave,

$$U_{ij}^{PS} = \mathrm{Re}\left\{ \begin{bmatrix} is\eta_\beta & \eta_\alpha\eta_\beta \\ -s^2 & is\eta_\alpha \end{bmatrix} \frac{Q(s)}{R(s)} \frac{ds}{dt} \right\}. \tag{4.11}$$

U_{ij}^{SS} is the displacement tensor for an incident S-wave producing a reflected S-wave,

$$U_{ij}^{SS} = \mathrm{Re}\left\{ \begin{bmatrix} \eta_\beta & -is \\ is & s^2/\eta_\beta \end{bmatrix} \frac{S(s)}{R(s)} \frac{ds}{dt} \right\}. \tag{4.12}$$

U_{ij}^{SP} is the displacement tensor for an incident S-wave yielding a

reflected P-wave,

$$U_{ij}^{SP} = \mathrm{Re}\left\{ \begin{bmatrix} is\eta_\beta s^2 & s^2 \\ -\eta_\alpha \eta_\beta & is\eta_\alpha \end{bmatrix} \frac{Q(s)}{R(s)} \frac{ds}{dt} \right\} . \tag{4.13}$$

U_{ij}^{SPS} is the displacement tensor for a incident S-wave, yielding a surface P-wave, and a reflected S-wave,

$$U_{ij}^{SPS} = \mathrm{Re}\left\{ \begin{bmatrix} \eta_\beta & -is \\ is & s^2/\eta_\beta \end{bmatrix} \frac{S(s)}{R(s)} \frac{ds}{dt} \right\} . \tag{4.14}$$

where

$$\begin{aligned} \eta_\alpha &= (s^2 - 1/c_1^2)^{1/2} \\ \eta_\beta &= (s^2 - 1/c_2^2)^{1/2} \\ Q(s) &= 4is(2s^2 - 1/c_2^2) \\ R(s) &= (2s^2 - 1/c_2 2)^2 - 4s^2\eta_\alpha\eta_\beta \\ S(s) &= 4is(2s^2 - 1/c_2 2) \end{aligned} \tag{4.15}$$

From the Cagniard method, there is a functional relationship between s and t for each contribution, i.e.

For the PP term: $t = sx_1 + i\eta_\alpha(h+x_2)$ (4.16)

For the PS term: $t = sx_1 + i(\eta_\beta x_2 + \eta_\alpha h)$ (4.17)

For the SS term: $t = sx_1 + i\eta_\beta(h+x_2)$ (4.18)

For the SP term: $t = sx_1 + i(\eta_\alpha x_2 + \eta_\beta h)$ (4.19)

Equation (4.9) corresponds to Hudson's equations (7.66) and (7.67) where we have used a more compact notation. The five reflection terms in (4.9) correspond to the five standard reflected wave types as shown in Figure 4.2.

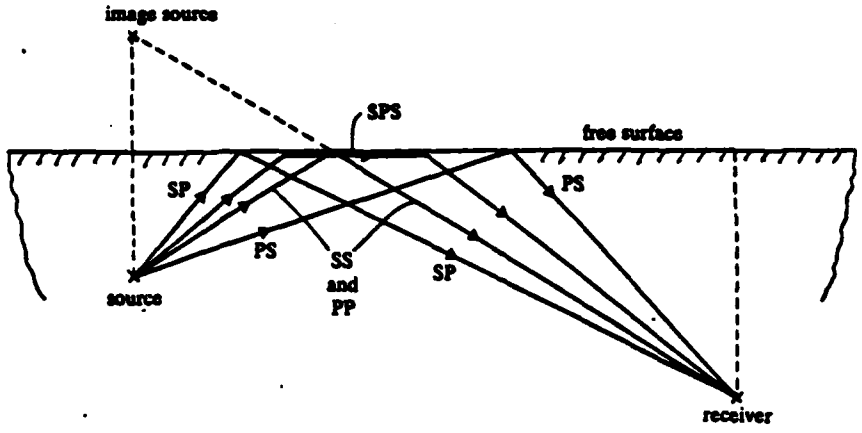

Fig. 4.2 The Ray Paths from Source to Receiver

As is common in problems of this type, some of the terms in relation (4.9) cannot be evaluated in closed form for a general field point below the boundary surface. For this case, the terms U_{ij}^{SP} and U_{ij}^{PS} are the ones which posses this problem. Through a Cagniard transformation, the quantity s must be determined by inverting the relations in equations (4.16)-(4.19). Equations (4.17) and (4.19) unfortunately do not lend themselves to simple inversions, and consequently a Newton root finding method for analytic functions was employed, see Rice [45] for details. For specified values of x_1, x_2 and t, the numerical routine computes s such that these equations will be satisfied. The derivative terms in equations (4.11) and (4.13) are computed by first employing implicit differentiation of relations (4.17) and (4.19) and then using the root finding values. This then allows direct computation of the U_{ij}^{SP} and U_{ij}^{PS} terms.

The stress field associated with this Green's function is computed

through Hooke's law to be

$$K_{ijk} = [\lambda\delta_{ij}\delta_{rs}+\mu(\delta_{ir}\delta_{js}+\delta_{is}\delta_{jr})]G_{rk,s} \tag{4.20}$$

4.4 Results for the Plane Strain Case

Specific results for the plane strain case were investigated for five points within the half-space as shown in Figures 4.3-4.6. The coordinate points are (0,5), (3,5), (5,5), (5,3), (5,0) all in cm. The Figures plot the non-dimensional Green's function $2c_2G_{ij}\pi\rho R$ versus dimensionless time c_2t/R, where R is the distance from the source to the receiver. The material properties chosen for use correspond to c_1 = 5800 m/s, c_2 = 3350 m/s and $\rho = 2.5\times10^3$ kg/m^3, and h = 10cm.

For the point (0,5) in Figures 4.3 and 4.4 the solid line is to be compared with the dots which represent the analytical solution by Payton [41]. Also for the point (5,0) in Figures 4.5 and 4.6, the solid line is compared with the dots which are the analytical solution results by Eringen and Suhubi [20]. As can be seen our results compare quite well to these analytical solutions for the special points considered.

The surface results at (5,0) as shown in Figures 4.5 and 4.6 initially presented a problem by not decaying properly after all the wave fronts had passed. This problem did not occur for the subsurface output in Figures 4.3 and 4.4. This decay problem was a result of a numerical instability that occurred when the individual reflection components were very large compared to the total sum. Each total displacement component should undergo monotonic decay with increasing time after all the wave fronts have gone by.

In order to resolve this instability problem a smooting operation was employed. After all the wave fronts have arrived, if instability (i.e. growth) was detected, the response was forced to decay at the same rate as an infinite space source problem with a similar receiver and time. The slope of this smoothing operation was made compatible by a linear interpolation of data points about the connecting data point. The infinite space solution was found in Eringen and Suhubi [20]. As can be seen in Figures 4.5 and 4.6 this procedure worked well and is only necessary at or near the free surface.

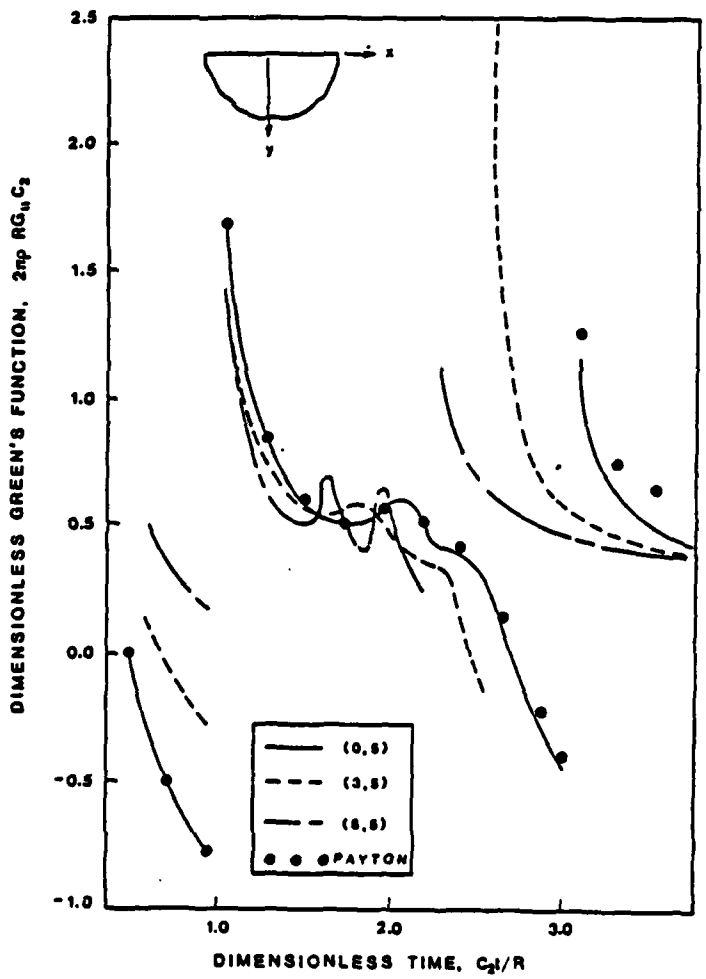

Fig. 4.3 Green's Function G_{11} and Comparison with Payton

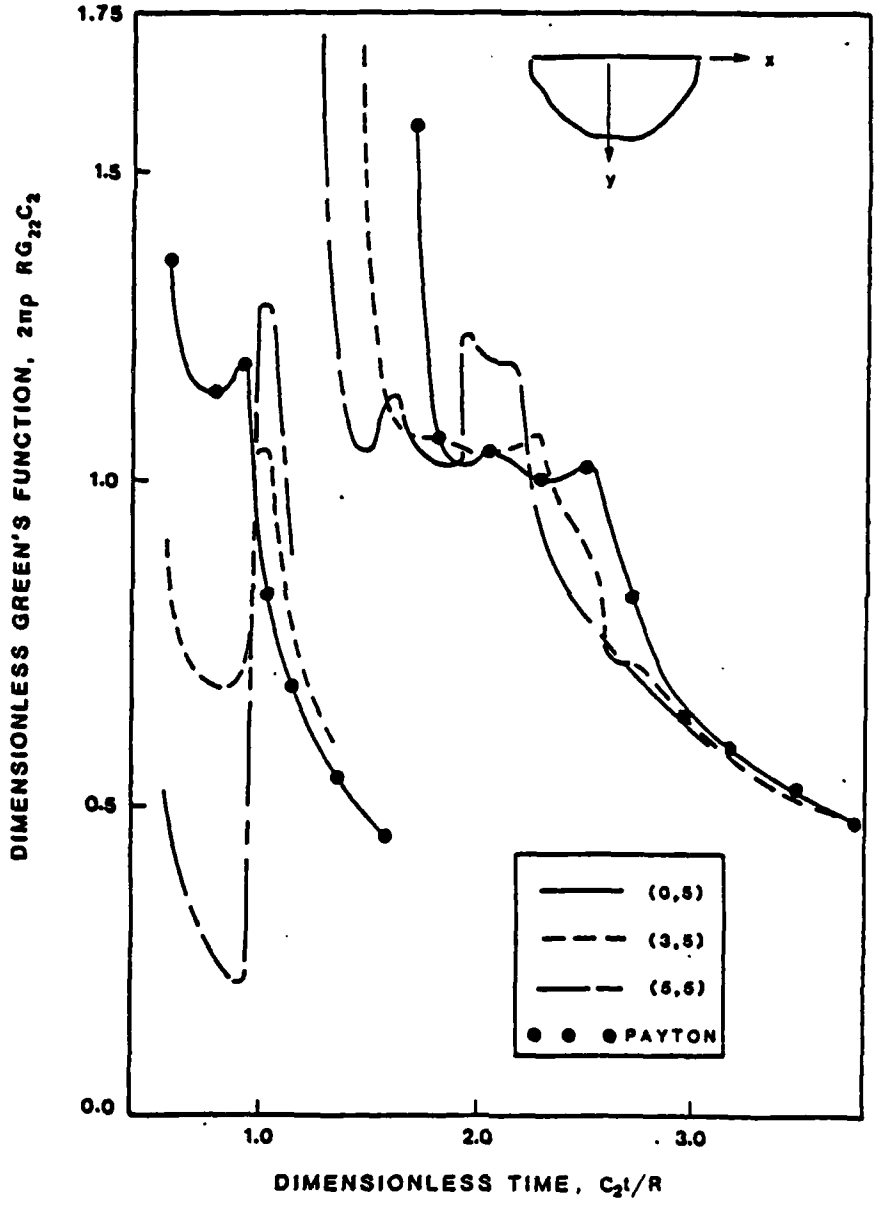

Fig. 4.4 Green's Function G_{22} and Comparison with Payton

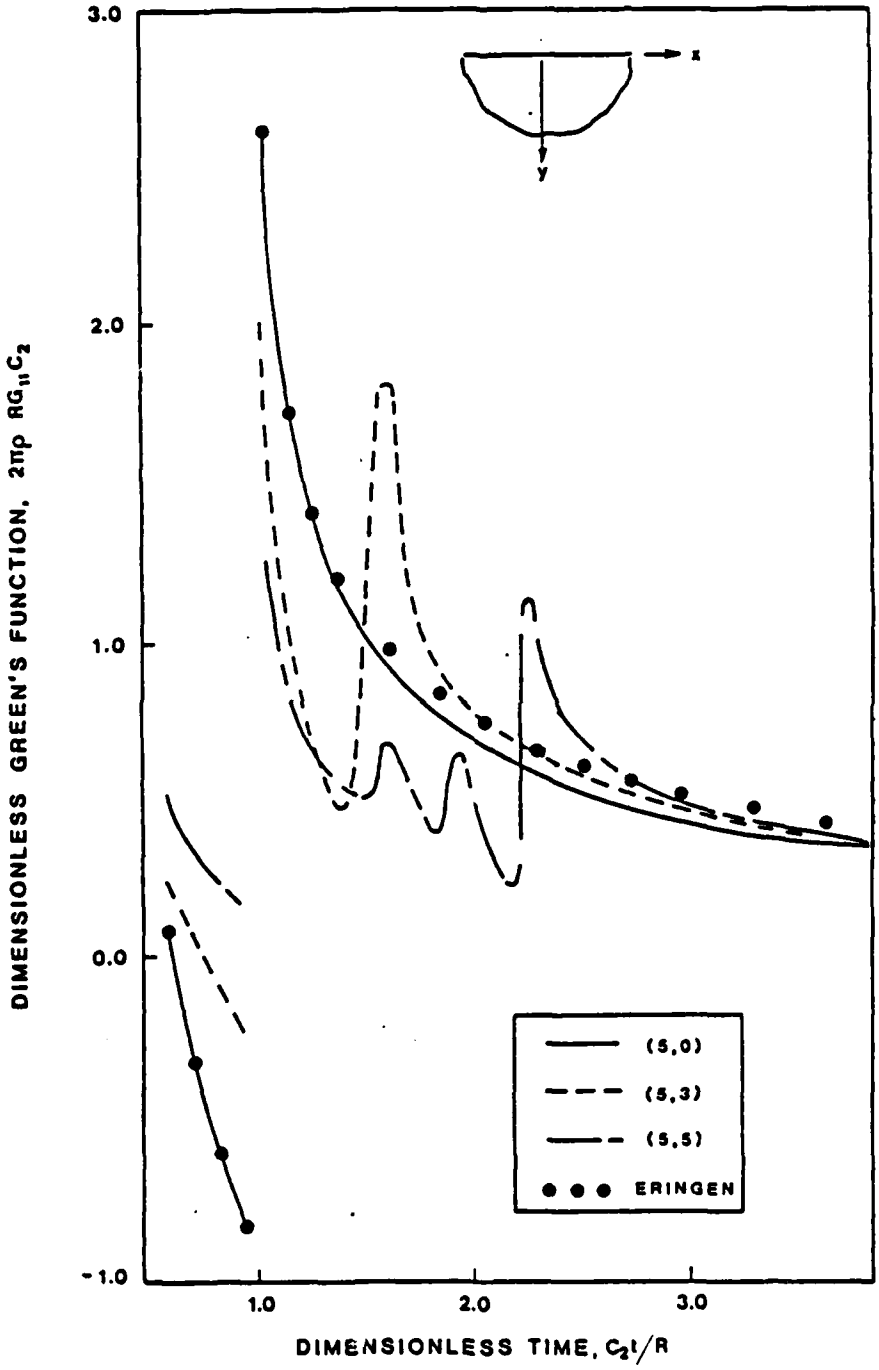

Fig. 4.5 Green's Function G_{11} and Comparison with Eringen

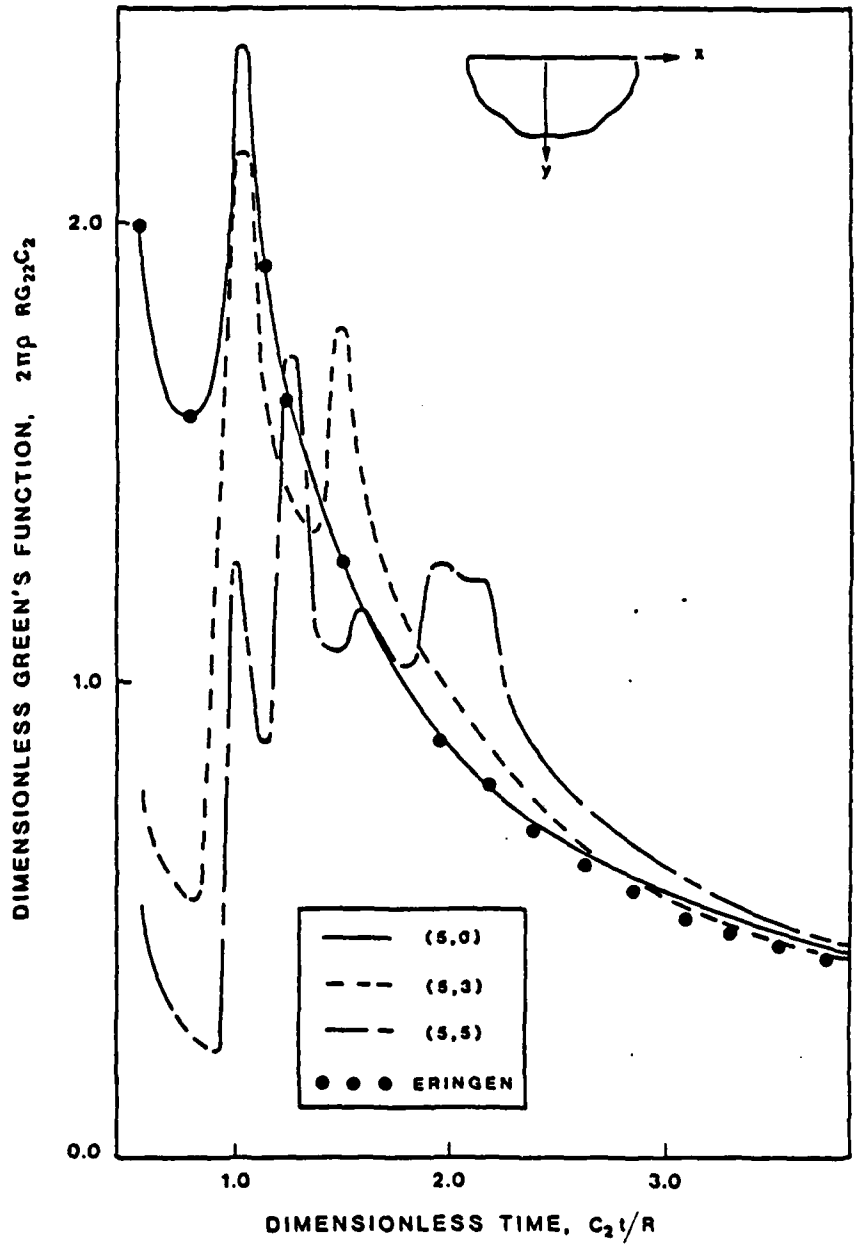

Fig. 4.6 Green's Function G_{22} and Comparison with Eringen

V ANTI-PLANE STRAIN WAVE MOTION

5.1 Introduction

This section is specifically concerned with developing a BEM technique for anti-plane strain using a time-dependent approach similar to that of Cole, et.al. [15]. The Green's function for the half-space geometry will be selected for use and this choice will eliminate the need to discretize the free surface of the half-space itself, thus reducing still further the number of required unknown variables. Attention will be directed to SH-waves propagating in a half-space with cavities or inclusions. The wave forms, cavity shape, size and number are all arbitrary.

5.2 Problem Formulation

The direct boundary integral equation method will be used to determine the solution of the anti-plane strain case for transient elastodynamic waves in an isotropic, homogeneous half-space. Recall that anti-plane strain is characterized by a displacement field of the form $\underline{u} = \{0,0,w(x_1,x_2)\}$. The non-zero component w satisfies the classical wave equation from (2.19), i.e.

$$w_{,ii} = \frac{1}{c_2^2}\ddot{w}, \tag{5.1}$$

where c_2 is the shear wave velocity, and the body forces are neglected.

From equation (2.32) the integral representation for anti-plane strain was given by

$$cw(\underline{r},t) = \int_0^\infty \int_{\partial S} [G\tau(\underline{r}_o,t_o) - w(\underline{r}_o,t_o)\underline{K}\cdot\underline{n}]dS(\underline{r}_o)dt_o \tag{5.2}$$

Equation (4.5) provides the proper Green's function, i.e.

$$G = \frac{1}{2\pi\mu}\left\{\frac{H(t-t_o-R_o/c_2)}{[(t-t_o)^2-R_o^2/c_2^2]^{1/2}} + \frac{H(t-t_o-R_1/c_2)}{[(t-t_o)^2-R_1^2/c_2^2]^{1/2}}\right\} \quad (5.3)$$

and the associated stress field is given by (4.6) to be

$$\underline{K} = \frac{1}{2\pi c_2^2}\left\{\frac{R_o H(t-t_o-R_o/c_2)}{[(t-t_o)^2-R_o^2/c_2^2]^{3/2}}\frac{\partial R_o}{\partial \underline{n}} + \frac{R_1 H(t-t_o-R_1/c_2)}{[(t-t_o)^2-R_1^2/c_2^2]^{3/2}}\frac{\partial R_1}{\partial \underline{n}}\right\} \quad (5.4)$$

Results (5.3) and (5.4) can now be used with equation (5.2) to construct a boundary integral equation to discretize and solve for the displacements and tractions on the boundaries. With the boundary data determined, equation (5.2) can be reapplied to find the displacements and stresses at any interior points. To solve for the stress at interior points, relation (5.2) is substituted into (2.18) yielding

$$\tau_{3i} = \mu\left\{\int_0^\infty \int_{\partial S} [G\tau(\underline{r}_o,t_o)-w(\underline{r}_o,t_o)\underline{K}\cdot\underline{n}]dS(\underline{r}_o)dt_o\right\}_{,i} \quad (5.5)$$

5.3 Numerical Discretization

The integral equation (5.2) must now be discretized in some manner in order to model a physical problem. For this case, the boundary to be integrated over was divided into elements with a node at the center of each. Each individual element is assumed to possess a constant displacement and a constant traction with respect to space. Integration over time was constant for the displacement kernel and linear for the stress kernel. Integration over a particular time step and space increment requires special attention. Rice [45] gives a description of the integration of the kernels with special emphasis on the

singularities. This was essentially the same scheme used by Cole [14]. It should be pointed out that it is possible to interpolate the variation of the dynamic variables over an element with any order of shape function (e.g. constant, linear, quadratic, etc.).

For a receiver point on the boundary, equation (5.2) thus becomes

$$\frac{1}{2} w_i^m + \sum_{n=1}^{m} \sum_{j=1}^{H} \int_{t_n} \int_{\Gamma_j} \underline{K}\cdot\underline{n}\, \phi_j^n (\underline{r}_o, t_o) w_j^n \, d\Gamma_o dt_o$$
$$= \sum_{n=1}^{m} \sum_{j=1}^{H} \int_{t_n} \int_{\Gamma_j} G\, \psi_j^n (\underline{r}_o, t_o) \tau_j^n \, d\Gamma_o dt_o \qquad (5.6)$$

where H is the total number of elements, and M is the total number of time increments. The receiver time is incremented by m, i.e. $t_m = m\Delta t$, m = 1,2,...M, while the source time is incremented by n, $t_n = n\Delta t$, n = 1,2,...M. The source boundary has H elements, and there are H receiver elements. Note that since a source time t_n cannot be greater than the receiver time, n is summed only up to m. ϕ_j^n and ψ_j^n are the interpolation functions for displacement and traction respectively.

Defining the discrete kernels or influence coefficients

$$IG_{ij}^{mn} = \int_{t_n} \int_{\Gamma_j} G\, d\Gamma_o dt_o$$

$$IK_{ij}^{mn} = \int_{t_n} \int_{\Gamma_j} \left[1 - \frac{(t_o - t_m)}{\Delta t}\right] \underline{K}\cdot\underline{n}\, d\Gamma_o dt_o,$$

equation (5.6) can be written as

$$\frac{1}{2} w_i^m + \sum_{n=1}^{m} \sum_{j=1}^{H} IK_{ij}^{mn} w_j^n = \sum_{n=1}^{m} \sum_{j=1}^{H} IG_{ij}^{mn} \tau_j^n \,. \qquad (5.7)$$

Equation (5.7) will yield a set of H linear algebraic equations to be solved at each time step. The final result of this will be the tractions and displacements of all the boundary elements at all the time steps.

Although there are $2H^2M^2$ possible kernels, not all need to be calculated as the Green's function has the time translation property,

$$G(\underline{r},t;\underline{r}_o,t_o) = G(\underline{r},t+\Delta t;\underline{r}_o,t_o+\Delta t) \tag{5.8}$$

and the causality property

$$G(\underline{r},t;\underline{r}_o,t_o) = 0 \quad \text{for} \quad c_2(t-t_o)<|\underline{r}-\underline{r}_o| \tag{5.9}$$

These properties greatly reduce the number of non-zero kernels in a given computational problem. Furthermore it is interesting to note that this discretization scheme can be implicit or explicit depending on the time spacing and the size of the elements. If $c_2\Delta t \leq \Delta h/2$, where h is the smallest element length, the coefficient matrix of the linear algebraic system to be solved will be diagonal and the discretization scheme will be explicit. If $c_2\Delta t > \Delta h/2$, the matrix will no longer be diagonal and the discretization scheme will be implicit. The integral equation is exact so any errors are a result of numerical integration. The surface of the body is discretized into small line segments and as one would expect the smaller the line segments the more accurate the surface representation andthe more accurate a solution. Integration of the Green's function in time has dominant errors near the singularities. These singularities occur when the direct wave or reflected wave just reaches the receiver point, as can be seen in the equation for the Green's function (5.3). As discussed in Cole [14], smaller time steps in general will give better accuracy. The problem with using smaller time steps is that one will need a larger number of time increments to get a suitable displacement output and there is a buildup of roundoff error

with each new time step.

In the case of an interior point, the displacement and stress can be solved for directly, once the boundary data is known, using the equations

$$w_p^m = \sum_{n=1}^{m} \sum_{j=1}^{H} IK_{pj}^{mn} w_j^n + \sum_{n=1}^{m} \sum_{j=1}^{H} IG_{pj}^{mn} \tau_j^n \tag{5.10}$$

$$\tau_{p(L)}^m = \mu[- \sum_{n=1}^{m} \sum_{j=1}^{H} IK_{pj}^{mn} w_j^n]_{,L} + [\sum_{n=1}^{m} \sum_{j=1}^{H} IG_{pj}^{mn} \tau_j^n]_{,L}$$

where, p is related to the interior point and L is the normal direction to the surface the stress is on.

5.4 Results

An example problem which will employ the solution method is shown in Figure 5.1, and contains a wave source and a stress free circular cavity embedded in an isotropic, homogeneous half-space. The geometry of the source was a four-sided square with an element on each side and the cavity was discretized into twelve elements. The distance between the source and cavity was held constant (ℓ = 0.1 m) while the depth of the source and cavity was varied (h = 0.05, 0.075, 0.1 m). The size of the source was 0.001 m wide and the cavity was 0.01 m in diameter. The mateial properties used corresponded to a shear wave speed of 3,200 m/s and a shear modules of 8.1 x 10^{10} N/m^2. The time increment was Δt= 2.5 x 10^{-6} s. Each configuration was run with the same input condition of a step displacement pulse of w_o= 0.01 m over the whole source boundary with a duration of one time increment.

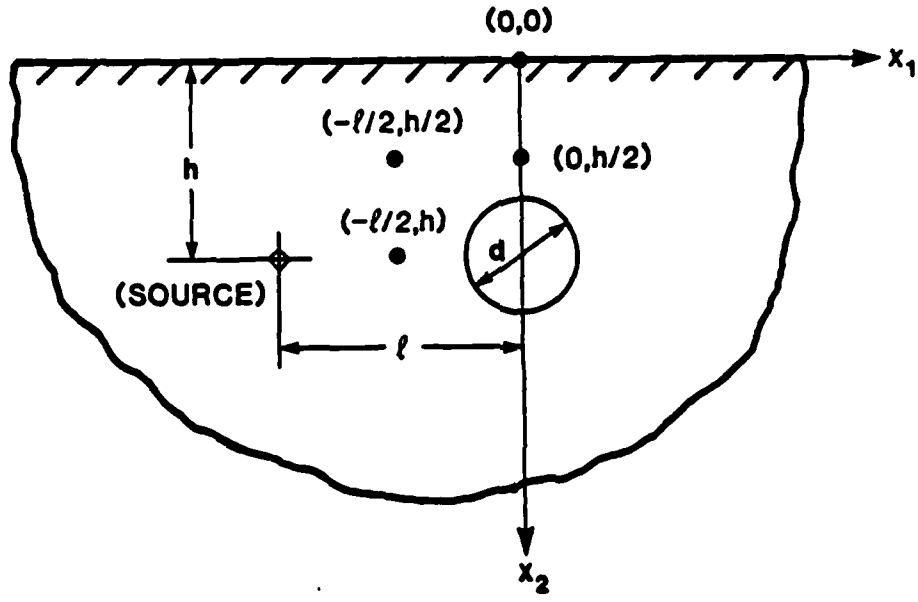

Fig. 5.1 Schematic of Buried Hole Problem

The resulting displacements from the above example were computed at four field received points (shown in Figure 5.1). Figure 5.2 illustrates the displacement-time response of the receiver point on the surface of the half-space at the coordinates (0,0). There is a distinct peak as the wave reaches this point. The closer the source to the receiver the greater the magnitude of the peak.

In Figure 5.3 the receiver point is half way between the cavity and the free surface at coordinates (0,h/2). In addition to the peaks from the direct wave there are now peaks from the reflection from the free surface, reflection from the cavity and reflection from the free surface via the cavity. Note, at $h/\ell = 0.5$ the events of the reflection from the free surface and reflection from the cavity should occur at approximately the same time according to ray theory. In general the longer the ray path the smaller the peak magnitude of the event. This, however, may not be the case near the free surface of the cavity or near the surface of

the half-space. Figure 5.4 corresponds to the receiver point at coordintes $(-\ell/2,h/2)$ and again illustrates several wave arrivals.

In Figure 5.5 the receiver point is located between the source and the cavity at coordinates $(-\ell/2,h)$. The direct waves for the various h/ℓ cases all occur at the same time with essentially identical magnitudes. For the $h/\ell = 1.0$ and 0.75 cases, the reflections from the cavity both occur at the same time with approximatey the same magnitude. Reflections from the cavity for the $h/\ell = 0.5$ case are associated with a larger displacement magnitude because of the presence of the free surface reflected wave.

These computer runs were made on a Prime 750 minicomputer, and a typical run used a total of 16 elements with 4 output points and 40 time steps. This resulted in a total run time of 6.5 cpu(s).

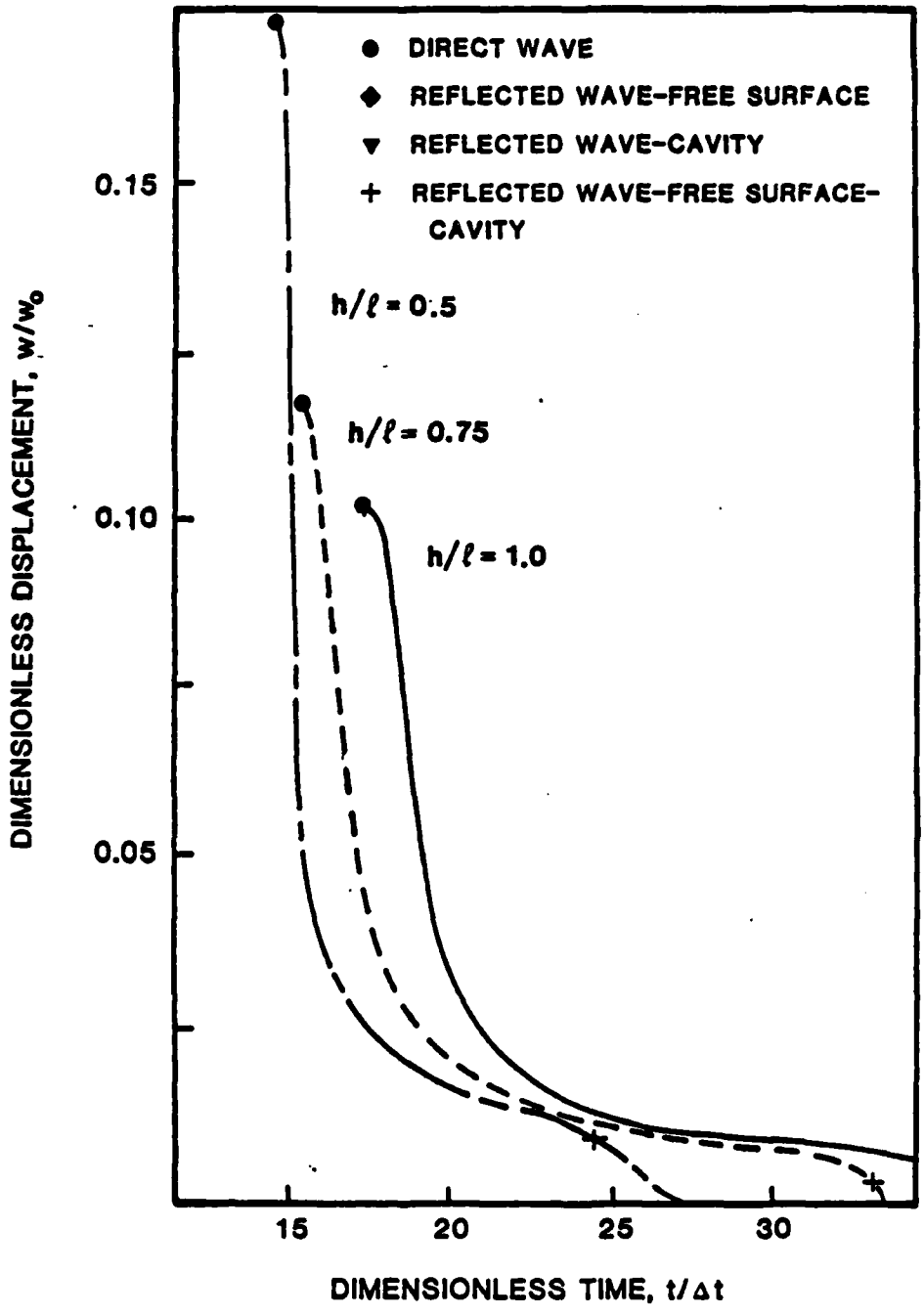

Fig. 5.2 Results of Buried Hole Problem at (0,0)

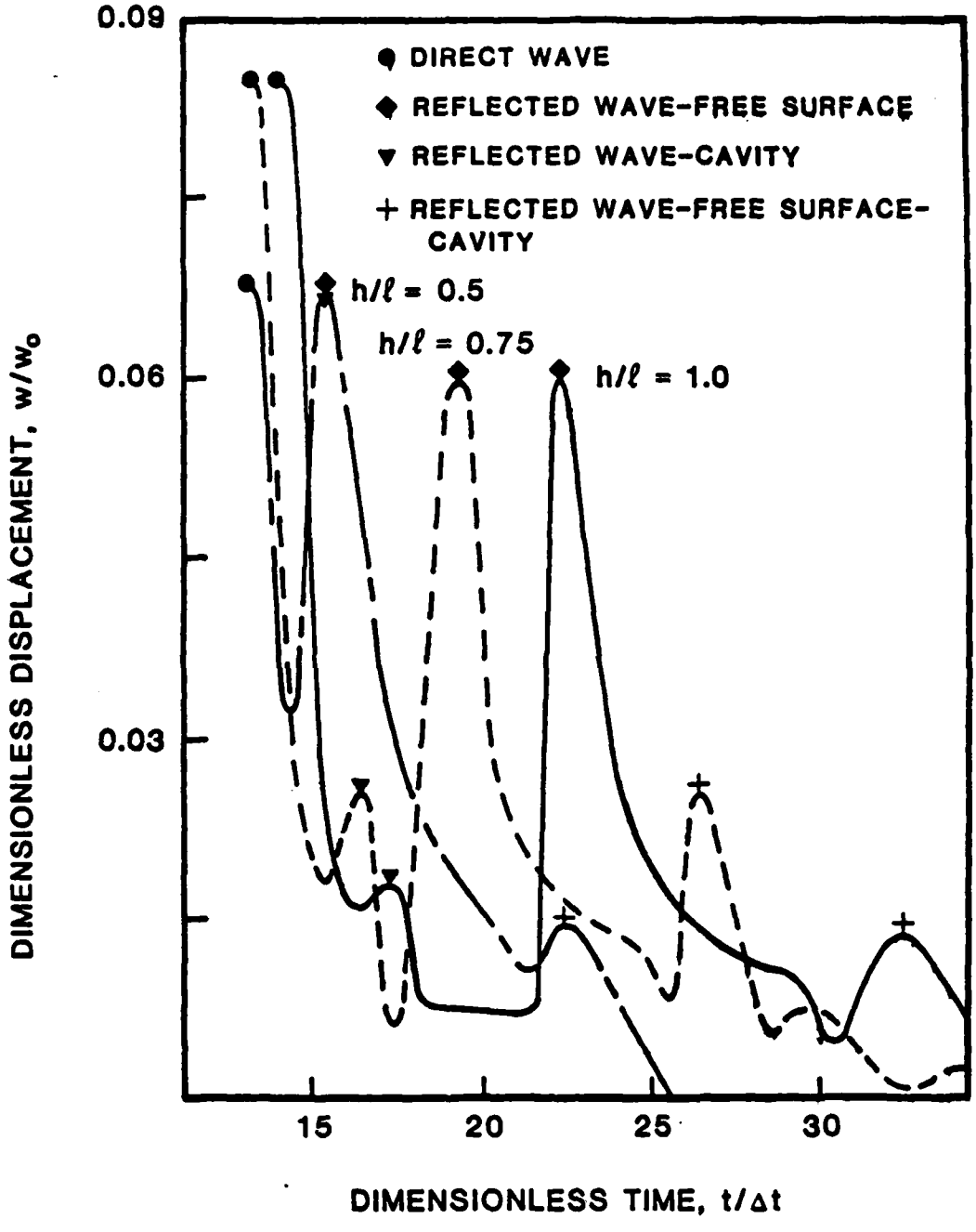

Fig. 5.3 Results of Buried Hole Problem at (0,h/2)

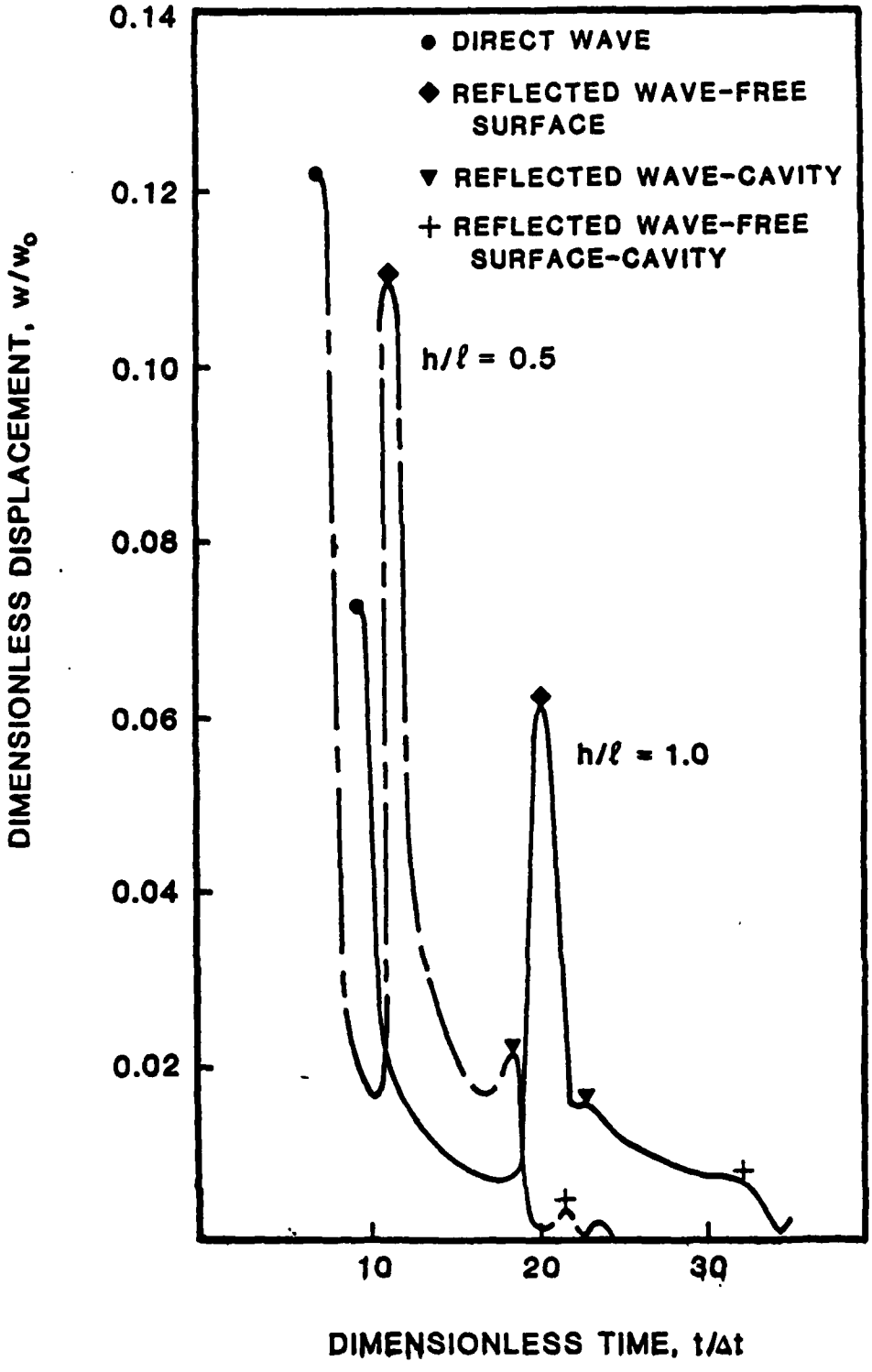

Fig. 5.4 Results of Buried Hole Problem at (-ℓ/2,h/2)

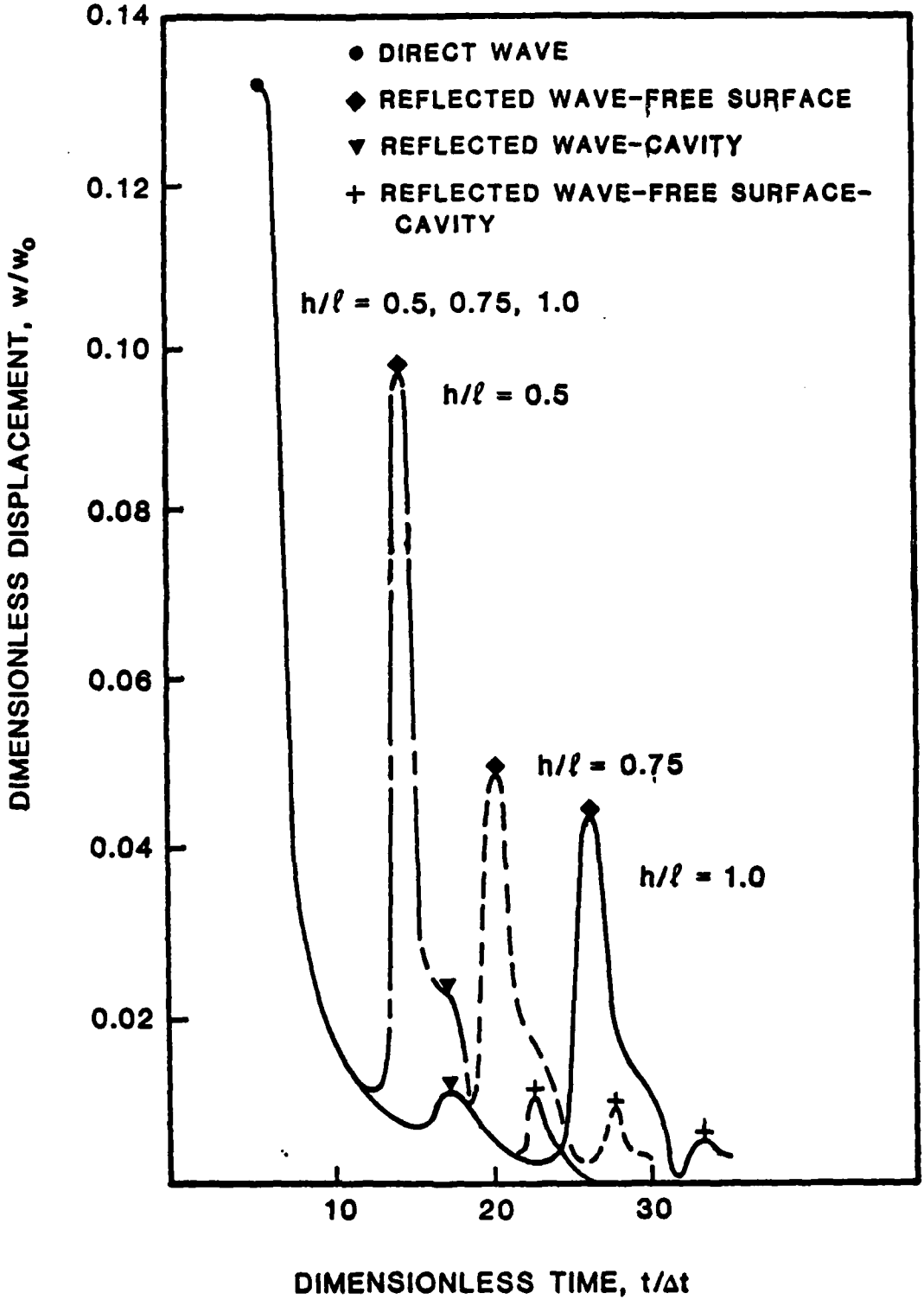

Fig. 5.5 Results of Buried Hole Problem at (-ℓ/2,h)

VI PLANE STRAIN WAVE MOTION

6.1 Introduction

This section is concerned with developing a BEM technique for plane strain elastodynamics using a time-dependent Green's function. As with the previous SH-wave case, the Green's function for the half-space geometry will be selected for use. This choice will again eliminate the need to discretize the free surface of the half-space itself, thus reducing the number of required unknown variables. Interest will be directed to SV-waves and P-waves propagating in a half-space with cavities or inclusions. The wave forms, cavity shape, size and number are all arbitray.

6.2 Problem Formulation

The direct boundary integral equation method will be used to determine the solution of the plane strain case for transient elastodynamic waves in an isotropic, homogeneous half-space. Plane strain is characterized by a displacement field of the form $\underline{u} = \{u(x_1,x_2) \ , \ v(x_1,x_2),0\}$. The equation of motion from (2.12) with zero body forces is given by

$$\mu\nabla^2\underline{u} + (\lambda+\mu)\underline{\nabla}(\underline{\nabla}\cdot\underline{u}) = \rho\ddot{\underline{u}} \ . \tag{6.1}$$

From equation (2.30) the integral representation for plane strain is

$$c\underline{u}(\underline{r}_o,t_o) = \int_0^\infty \int_{\partial S} [\underline{\underline{G}}\underline{\tau}(\underline{r},t)\cdot\underline{u}(\underline{r},t)\underline{\underline{K}}\cdot\underline{n}]dS(\underline{r})dt \ . \tag{6.2}$$

The Green's function for the plane strain half-space domain was developed in section 4.3, and is given by

$$G_{ij} = \frac{1}{2\pi\rho}\,[H(t-r''/c_1)U_{ij}^{PP} + H(t-t_{SP})U_{ij}^{SP} + H(t-t_{PS})U_{ij}^{PS}$$
$$+ H(t-r''/c_2)U_{ij}^{SS} + H(t-t_{SPS})H(r''/c_2-t)U_{ij}^{SPS} + H(t-r'/c_1)U_{ij}^{P}$$
$$+ H(t-r'/c_2)U_{ij}^{S}] \qquad (6.3)$$

where U_{ij}^{P}, U_{ij}^{S} corresponds to the incident field, and is given by Hudson [24]. The stress field associated with this Green's function is from (4.20)

$$K_{ijk} = [\lambda\delta_{ij}\,\delta_{rs} + \mu(\delta_{ir}\,\delta_{js} + \delta_{is}\,\delta_{jr})]G_{rk,s}\,. \qquad (6.4)$$

Results (6.3) and (6.4) can now be used with equation (6.2) to construct a boundary integral equation to solve for the displacements and tractions on the boundaries. With the boundary data determined, equation (6.2) can be reapplied to find the displacements at any interior points.

6.3 Numerical Discretization

The integral equation (6.2) must now be discretized in order to model a physical problem. Similar to the SH-wave case, the boundary to be integrated over was divided into elements with a node at the center of each. Each individual element is assumed to possess a constant displacement and a constant traction with respect to space and time. This differs slightly from the anti-plane strain case where the displacement was constant in space and linear in time. Because the

half-space Green's function is a system of waves (direct, reflective, and surface) it possesses multiple singularities in its values for a typical source/receiver pair at different times. Integration over a particular time increment in which a singularity appears, requires special attention. A Gauss four point quadrature was employed to integrate both in space and time. This allows one to sample points over the integral other than the endpoints which may be singular. Rice [45] gives a description of the integration of the kernals with special emphasis on the singularities.

For a receiver point on the boundary, equation (6.2) becomes

$$\frac{1}{2} w_i^m + \sum_{n=1}^{m} \sum_{j=1}^{H} \int_{t_n} \int_{\Gamma_j} \underline{\underline{K}} \, \phi_j^n (\underline{r},t) w_j^n \, d\Gamma dt$$
$$= \sum_{n=1}^{m} \sum_{j=1}^{H} \int_{t_n} \int_{\Gamma_j} \underline{\underline{G}} \, \psi_j^n (\underline{r},t) \tau_j^n \, d\Gamma dt \,, \tag{6.5}$$

where H, M, m, n, ϕ_j^n and ψ_j^n are the same as previously defined in section 5.3

Defining the discrete kernels or influence coefficients

$$IG_{ij}^{mn} = \int_{t_n} \int_{\Gamma_j} \underline{\underline{G}} \, d\Gamma_o dt_o$$

$$IK_{ij}^{mn} = \int_{t_n} \int_{\Gamma_m} \underline{\underline{K}} \, d\Gamma_o dt_o$$

equation (6.5) can be written as

$$\frac{1}{2} u_i^m + \sum_{n=1}^{m} \sum_{j=1}^{H} IK_{ij}^{mn} \, u_j^n = \sum_{n=1}^{m} \sum_{j=1}^{H} IG_{ij}^{mn} \, \tau_j^n \,. \tag{6.6}$$

Equation (6.6) will yield a set of H linear algebraic equations to be solved at each time step. The final result of this will be the tractions and displacements of all the boundary elements at all the time steps. Note, this closely resembles the scheme used for anti-plane strain; the difference being that $\underline{\underline{G}}$ and $\underline{\underline{K}}$ are now second order and third order tensors, respectively. Also, the integration is now over the receiver points. In the anti-plane strain case the integration was over the source points.

Although there are $8H^2M^2$ possible kernels, not all need to be calculated as the Green's function has the time translation property, (5.8) and the causality property (5.9). These properties greatly reduce the number of non-zero kernels in a given computational problem. Furthermore it is again interesting to note that this discretization scheme can be implicit or explicit depending on the time spacing and the size of the elements. If $c_1 \Delta t \leq h/2$, where h is the smallest element length, the discretization scheme will be explicit. If $c_1 \Delta t > \Delta h/2$, the discretization scheme will be implicit. This method works better for an implicit scheme where $\Delta t\ c_2$ is approximately equal to the diameter of the largest cavity. When $\Delta t\ c_2$ is less than the diameter of the largest cavity, the solution blows up or gets larger with increasing time. There appears to be a need for each element to receive influence from each of the other elements on a continuous surface.

In the case of an interior point, the displacement can be solved for directly, once the boundary data is known, i.e.

$$u_p^m + \sum_{n=1}^{m} \sum_{j=1}^{H} IK_{pj}^{mn}\, w_j^n = \sum_{n=1}^{m} \sum_{j=1}^{H} IG_{pj}^{mn}\, \tau_j^n \qquad (6.7)$$

where, p is related to the interior point.

6.4 Results

In section 4.4, a check of the plane strain half-space Green's function was made by comparing the result with the Payton [41] and Eringen [20] solutions. As a check of the total BEM scheme, a comparison was made between Garvin's analytical solution [22] and a BEM computer model. Garvin's work provides an exact solution for the surface response due to a buried dilatational line source of impulsive time dependence.

In trying to compare these two solutions it should be pointed out that there are basic unreasolvable differences between the Garvin solution and the BEM computer model. Garvin's solution is due to a buried line source excitation as represented in Figure 6.1. The radial

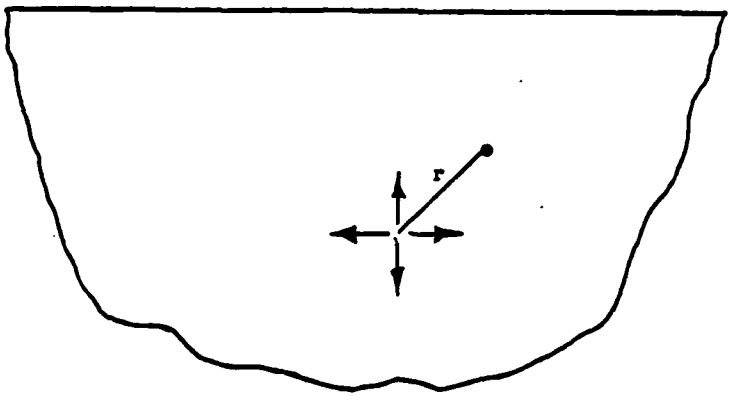

Fig. 6.1 Garvin Problem Configuration

displacement of the source is given by Garvin to be

$$u_r = \frac{at\ H(t-r/c_1)}{2r[t^2-(r^2/c_2{}^2)]^{1/2}}\ , \qquad (6.8)$$

where 'a' is a constant representing the source strength and r is the distance between the source and receiver point. This is taken to be an approximate representation of a pulse emitted by an explosion, and represents a sudden singular jump followed by a gradual incomplete recover, see Figure 6.2.

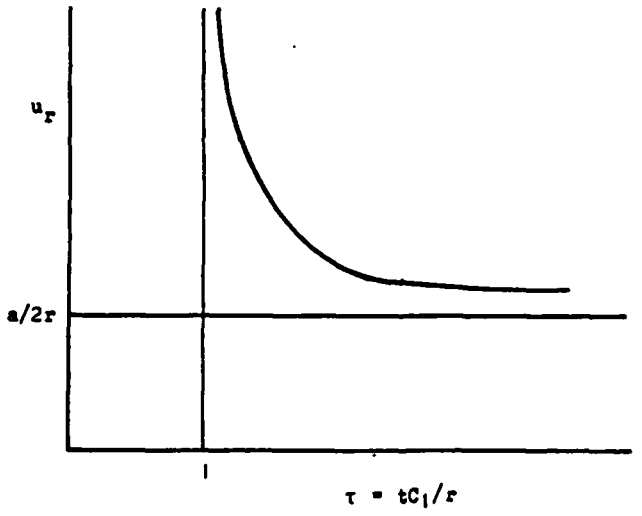

Fig. 6.2 Garvin Source Displacement Function

In contrast the BEM model incorporates a buried cavity of finite size as a source as shown in Figure 6.3. This buried source was modeled as an eight-sided cavity with a diameter of 0.005 m located at a depth of 0.1 m

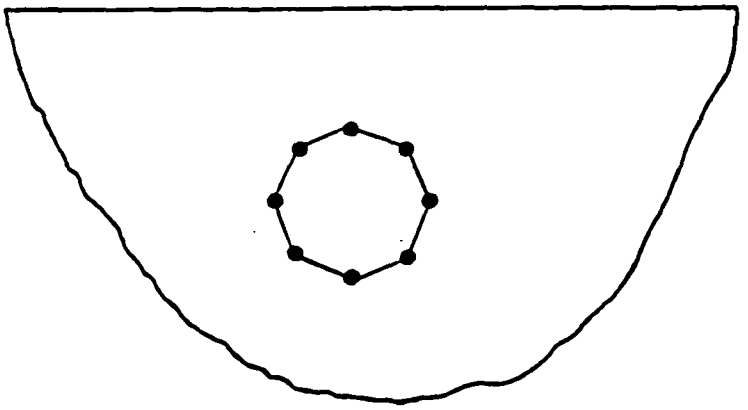

Fig. 6.3 BEM Source Configuration

in the half-space. On this buried cavity a radial traction boundary condition was used to represent the source excitation in Garvin's solution. The form of this traction function was

$$t_r = [\frac{6x10^{-4}}{t} + 600] \text{ Dynes}, \qquad (6.9)$$

and is plotted in Figure 6.4. Note, the function is not smooth as it is discretized to be constant over each time increment.

Therefore in order to alleviate the differences between the actual Garvin problem and the BEM model:

1. The cavity was made small with respect to its depth.

2. The Garvin solution was scaled by adjusting the source strength parameter 'a', to match the computer solution at a point below the surface near the cavity. A comparison was then made at various other points along the free surface.

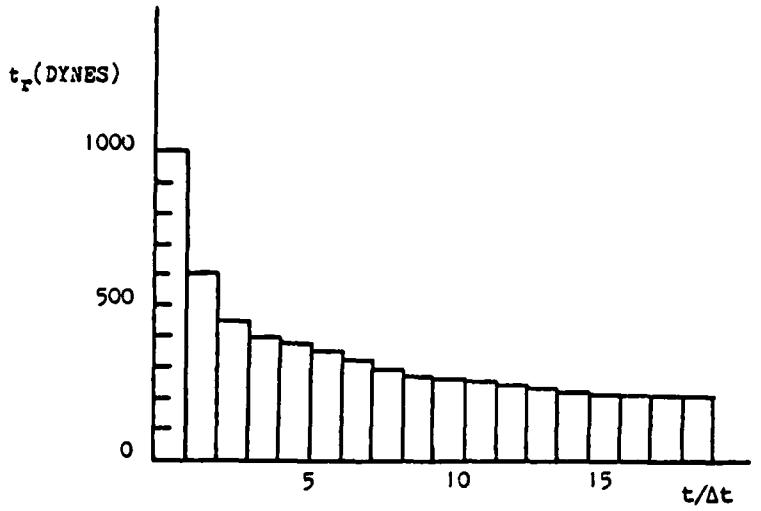

Fig. 6.4 BEM Boundary Traction Profile

Figure 6.5 shows the vertical displacement solution below the free surface at (0,7.5) cm. The value of 'a' in Garvin's solution was adjusted to be 1.3 x $10^{-10}cm^2$ to match the BEM solution. The material properties correspond to a P-wave speed of 5800 m/s, an S-wave speed of 3350 m/s, and a density of 2500 kg/m^3. Figure 6.5 shows both Garvin's source solution and the BEM solution with this value of 'a' for comparison. As shown in Figure 6.6, on the free surface, there is very good comparison directly above the buried source at (0,0). Reasonably good comparisons also exist at points farther away from the source as illustrated in Figures 6.7-6.10.

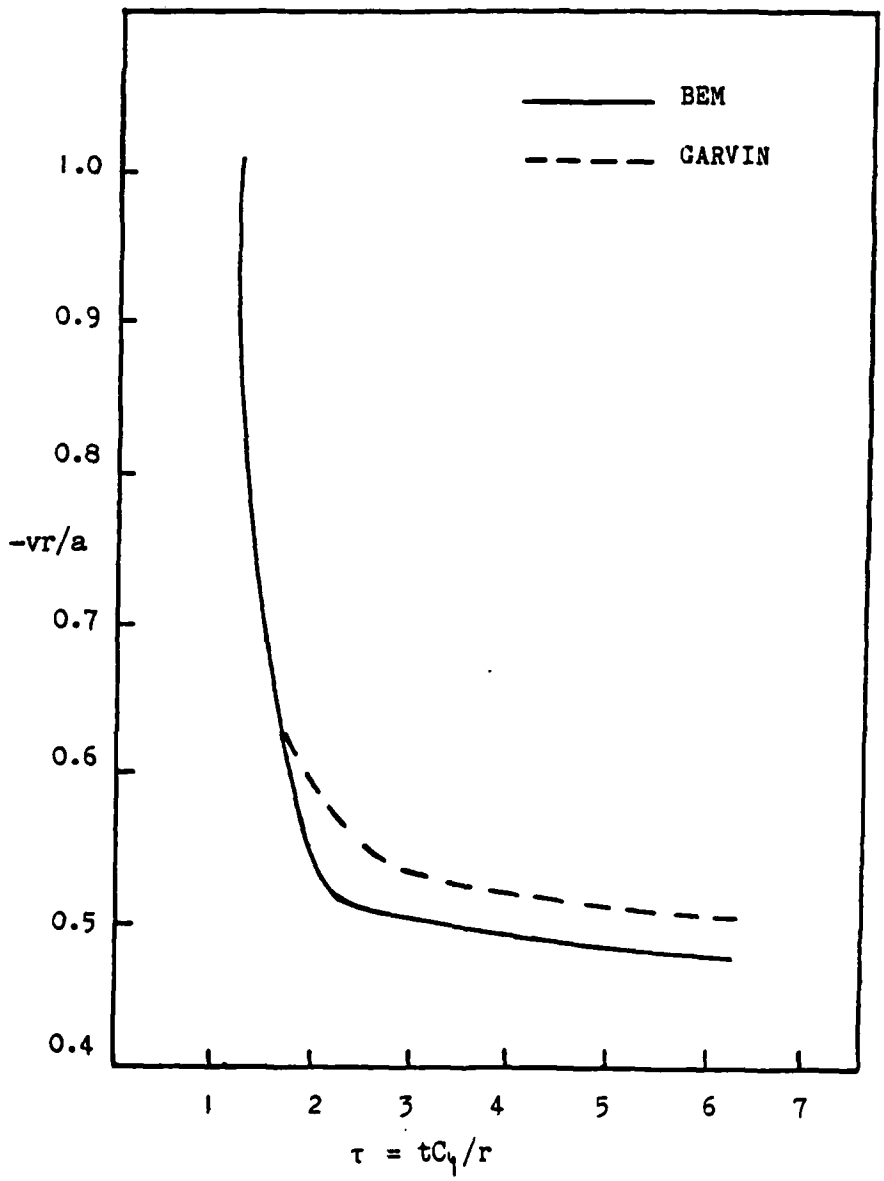

Fig. 6.5 Source Comparisons of the Vertical Displacement at (0,7.5)cm.

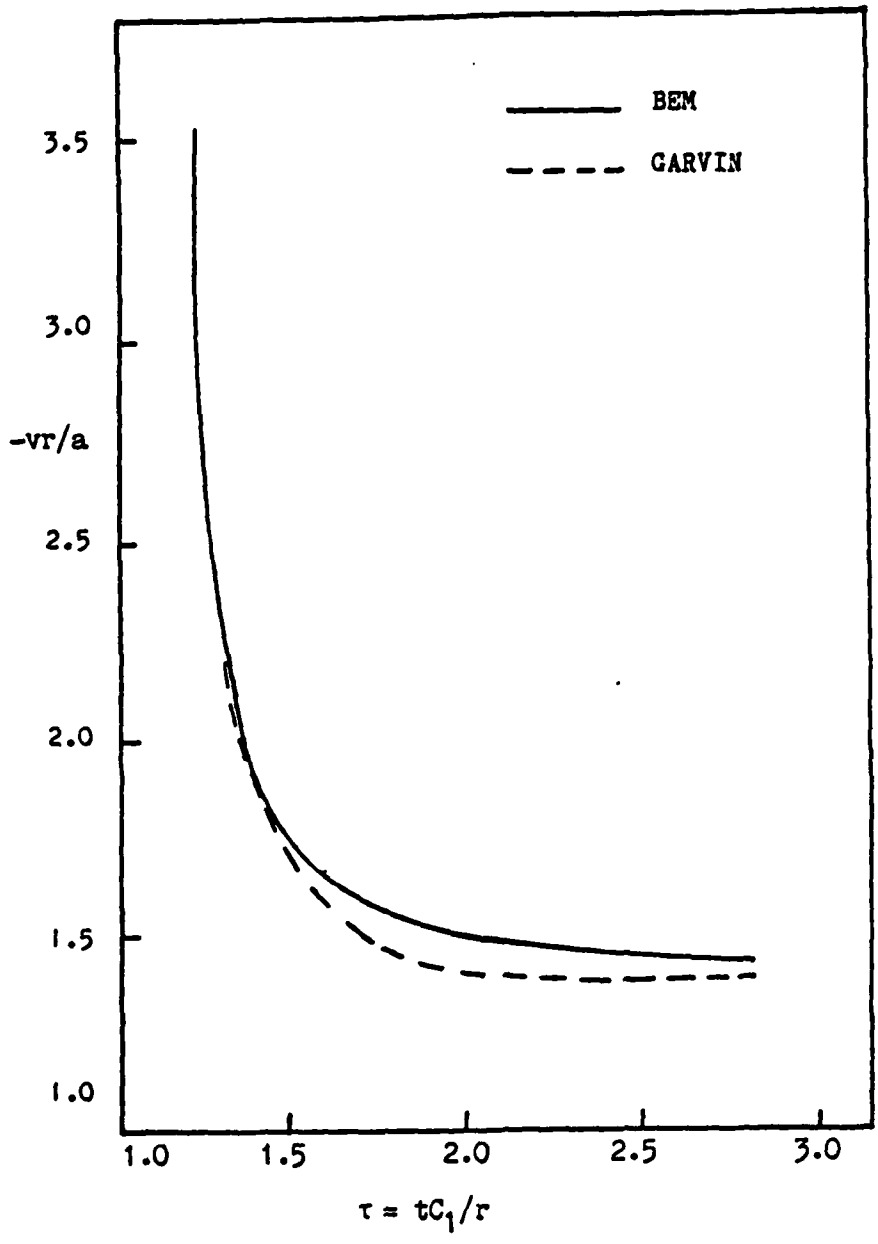

Fig. 6.6 Surface Vertical Displacement Comparison at (0,0)cm.

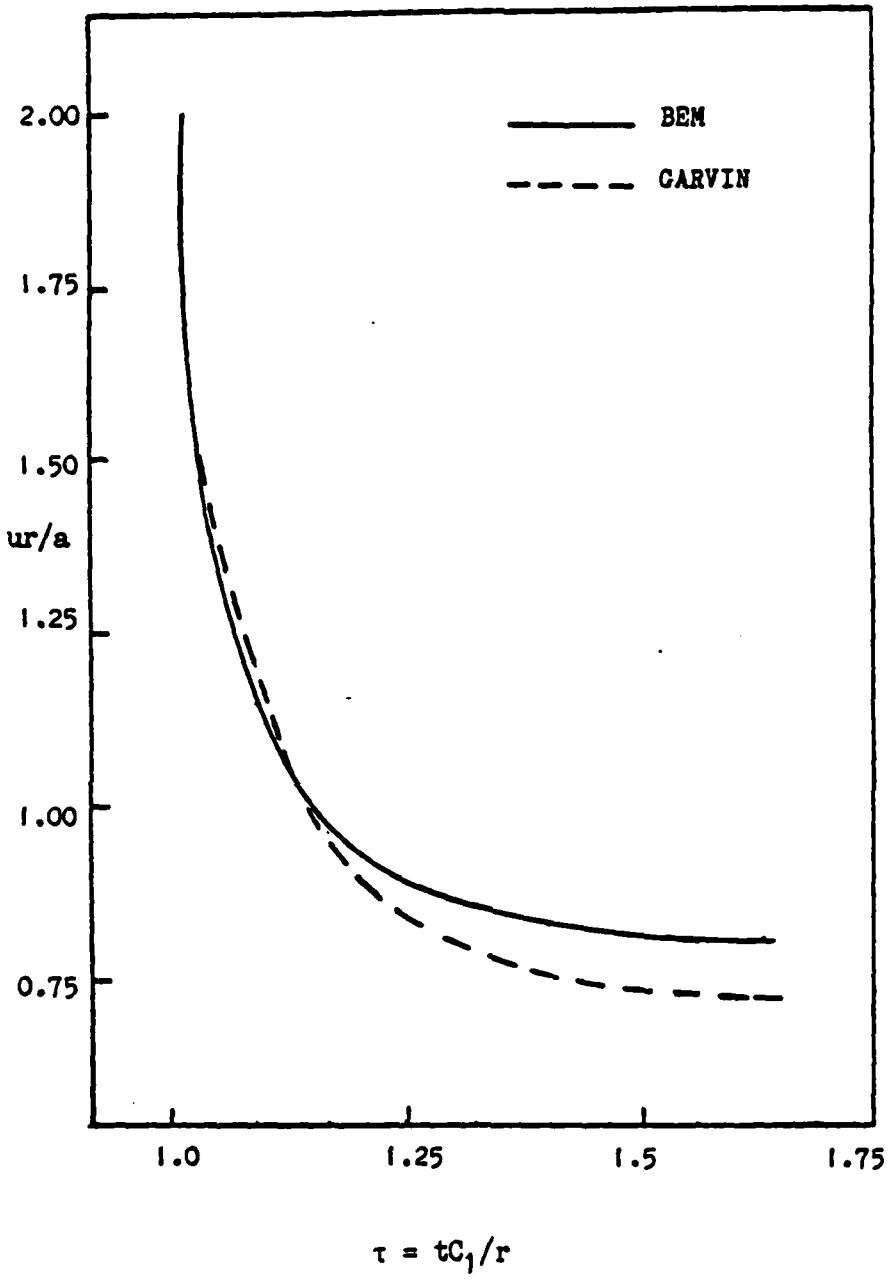

Fig. 6.7 Surface Horizontal Displacement Comparison at (5,0)cm.

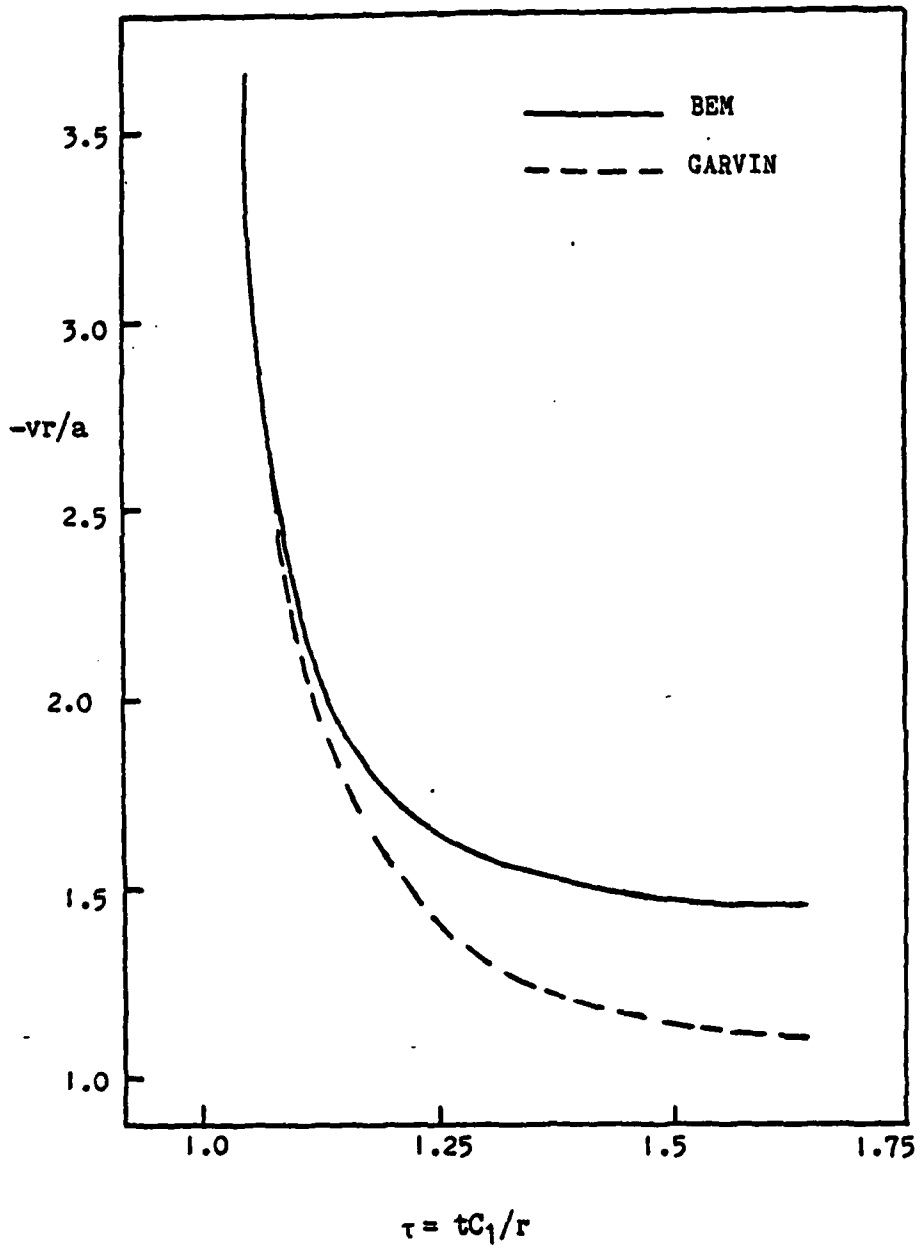

Fig. 6.8 Surface Vertical Displacement Comparison at (5,0)cm.

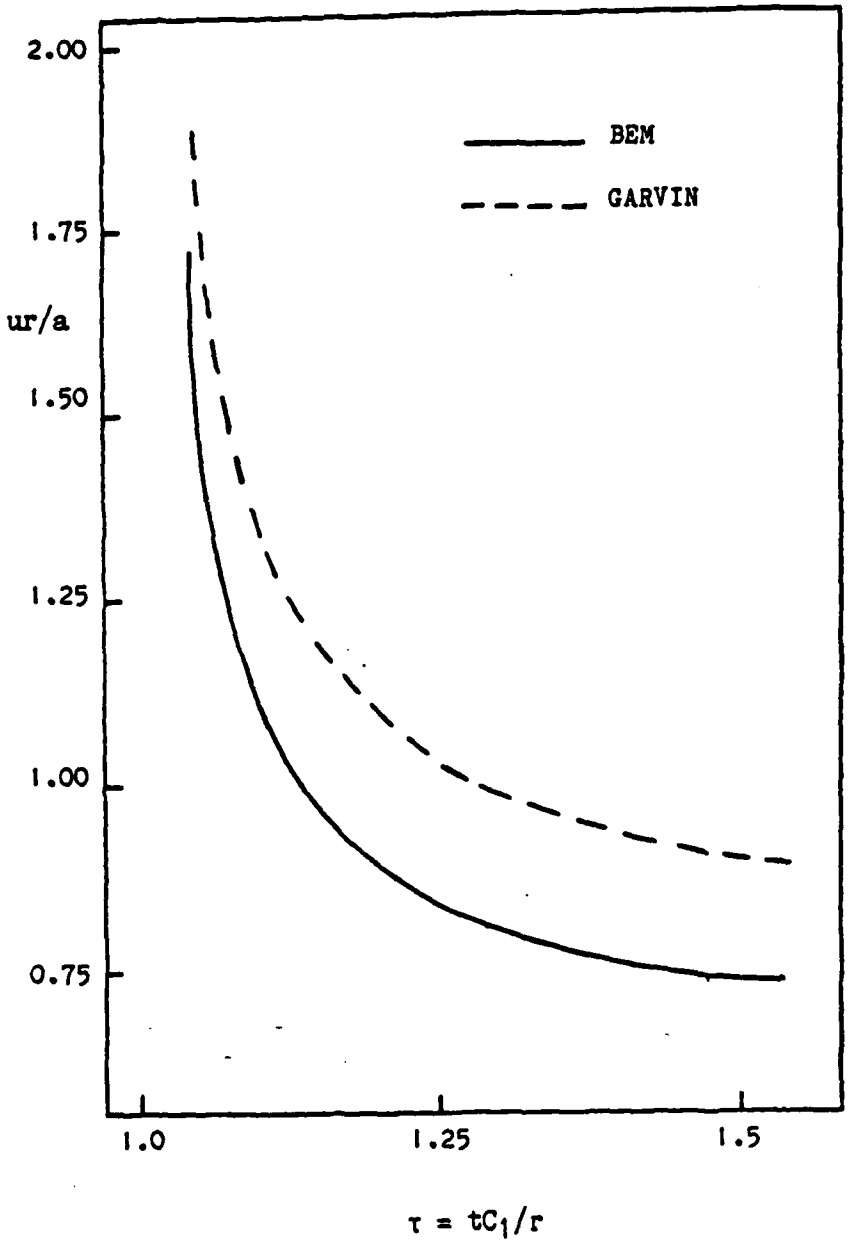

Fig. 6.9 Surface Horizontal Displacement Comparison at (10,0)cm.

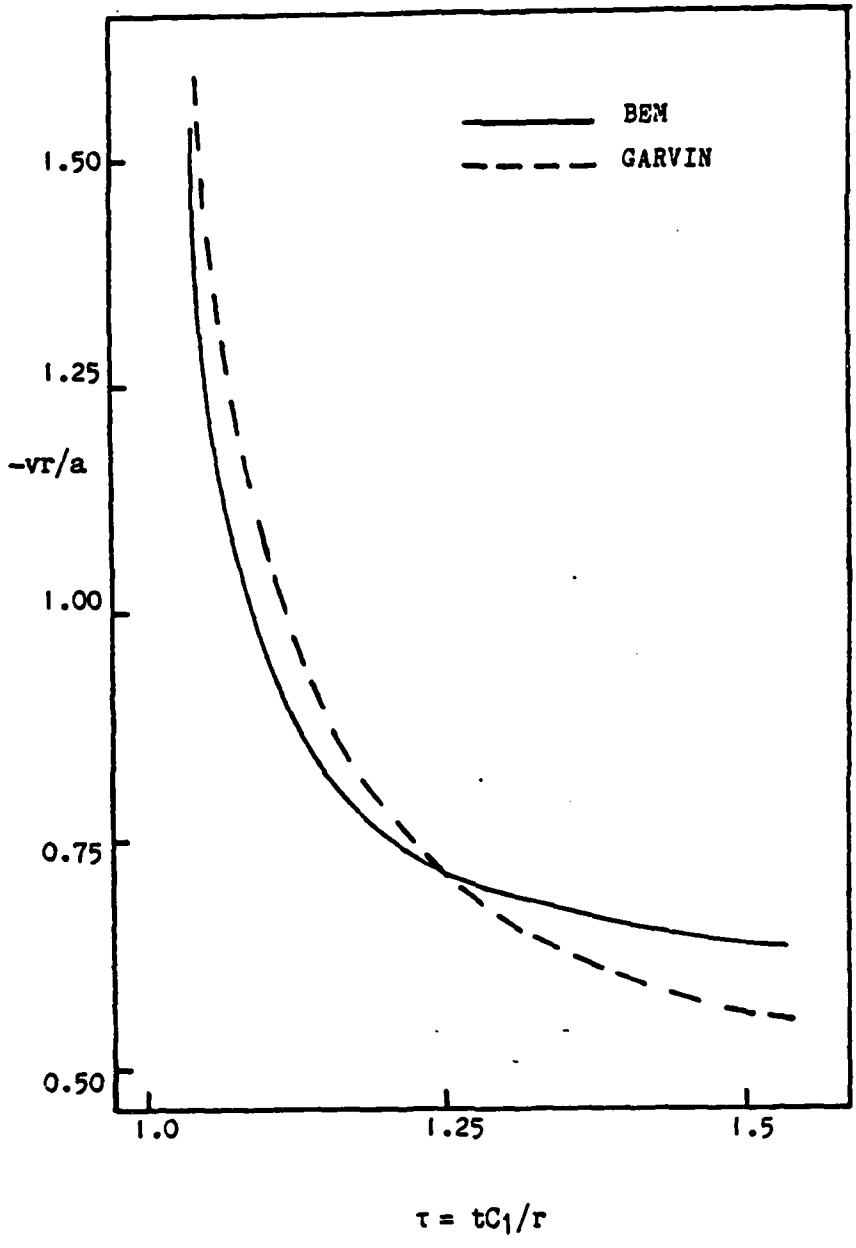

Fig. 6.10 Surface Vertical Displacement Comparison at (10,0)cm.

Another example problem which will employ the solution method is shown in Figure 6.11. The problem (similar to the SH-wave example) contains a wave source and a stress free circular cavity embedded in an isotropic, homogeneous half-space. The geometry of the source was a four sided square and the cavity was modeled as a twelve sided hole. The distance between the source and cavity was 0.1 m and the depth of the source and cavity was 0.1 m. The size of the source was 0.001 m wide and the cavity was 0.01 m in diameter. The material properties used corresponded to a P-wave speed of 5940 m/s and a S-wave speed of 3,200 m/s and a density of 7800 kg/m^3. The time increment was $\Delta t=3.2 \times 10^{-6}s$. This configuration was run with the input condition of a step normal displacement pulse of Δ_0= 0.001 m over the whole source boundary with a duration of one time increment.

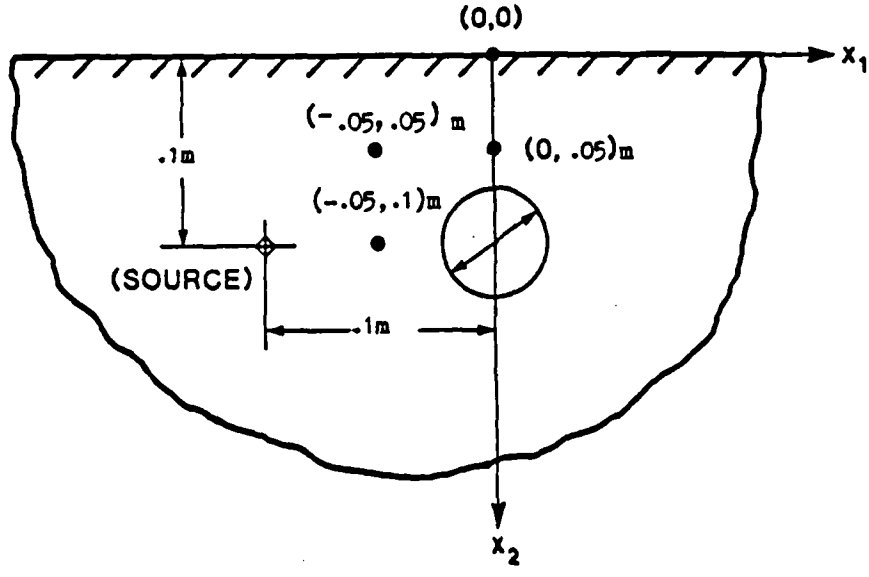

Fig. 6.11 Schematic of Buried Hole Problem

The resulting displacements from this example were computed at four field receiver points as shown in Figure 6.11. Figures 6.12-6.15 plot dimensionless displacement vs. dimensionless time. The dimensionless displacements u/Δ_0 and v/Δ_0 are the horizontal and vertical displacements repsectively, normalized by the initial step displacement magnitude. The dimensionless time $t/\Delta t$ is the actual time divided by the time increment. The notation in these four figures represent the events that occur as particular waves pass the receiver point. These waves are classified as

Direct Waves

- P: (Dilatation Wave)
- S: (Shear Wave)

Free Surface Reflected Waves

- PP: (Incident P-wave and reflected P-wave)
- PS: (Incident P-wave and reflected S-wave)
- SS: (Incident S-wave and reflected S-wave)
- SP: (Incident S-wave and reflected P-wave)

Surface Wave

- S-SP: (Incident S-wave which travels along the surface as P-wave)

Cavity Reflected Waves

- CR-P: (P-wave reflected from the cavity)
- CR-S: (S-wave reflected from the cavity)

Multiple Reflected Waves

-SCR-P: (P-wave reflected from the free surface and then from the cavity)

Figure 6.12 illustrates the displacement-time response of the receiver point on the surface of the half-space at the coordinates (0,0). There are relatively few events in this Figure since no reflected waves interact with this point. There are distinct peaks as the wave reaches this location and the S-wave and surface P-wave act together at the same time. Note, because the ray angle makes equal angles with the x_1 and x_2 axis, the horizontal and vertical displacements are approximately the same from the time the P-wave passes until another event takes place.

In Figure 6.13 the receiver point is half way between the cavity and the free surface at coordinates (0,5) cm. There are more events as reflections from the free surface and the buried cavity are observed. Note, the horizontal displacements are relatively larger than the vertical displacements, due to the shallow angle between the source and receiver point. Figure 6.14 corresponds to the receiver point at coordinates (-5,5) cm. and again illustrates several wave arrivals. Again because of geometry, the horizontal and vertical displacements are approximately equal from the time the P-wave passes until another event takes place. In Figure 6.15 the receiver is located between the source and the cavity at coordinates (-5,10)cm. Note, the vertical displacement is zero until reflections occur.

A typical computer run of 16 elements with 4 output points and 30 time steps, results in a run time of approximately 50 cpu(m).

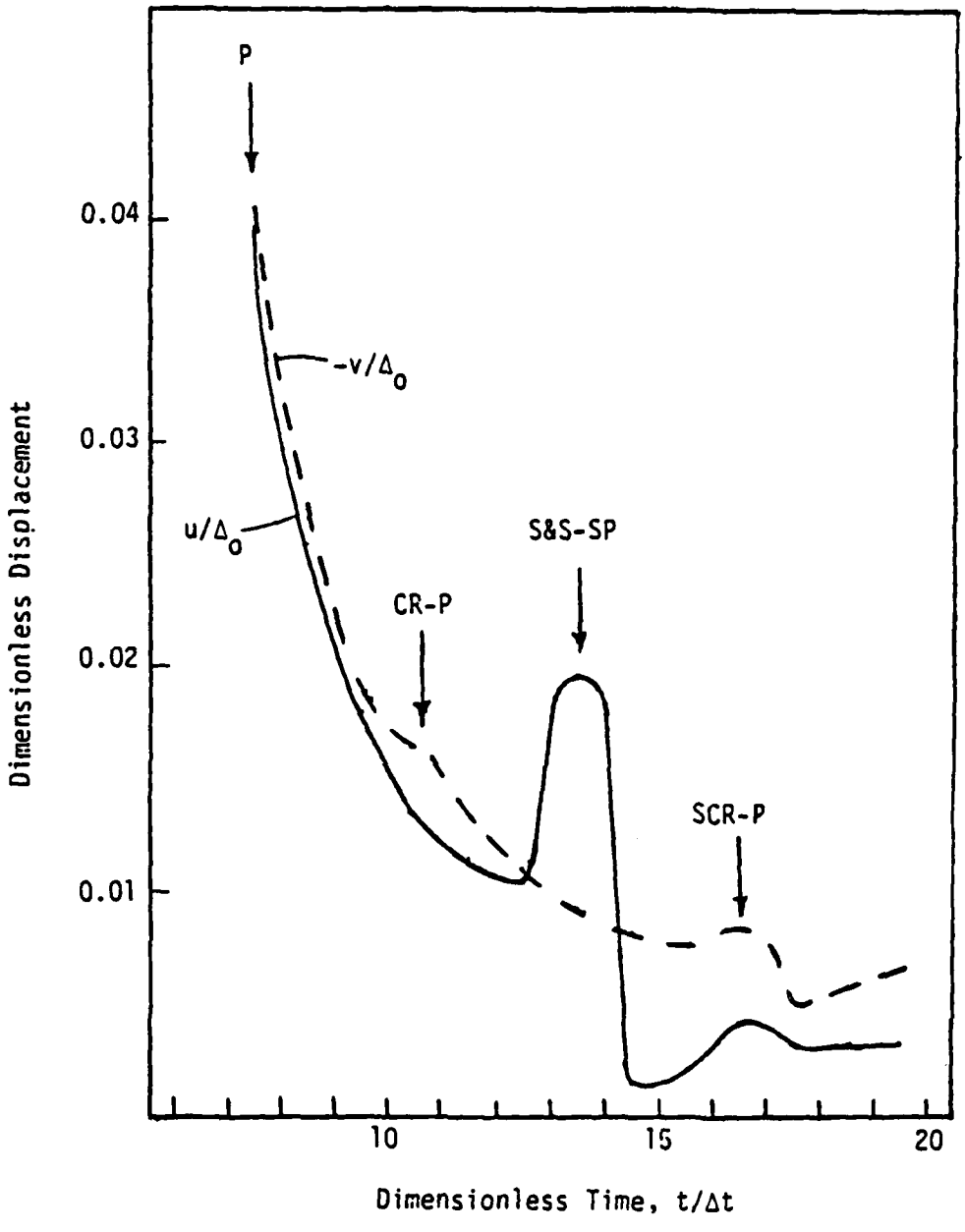

Fig. 6.12 Plane Strain Displacement Response at (0,0)

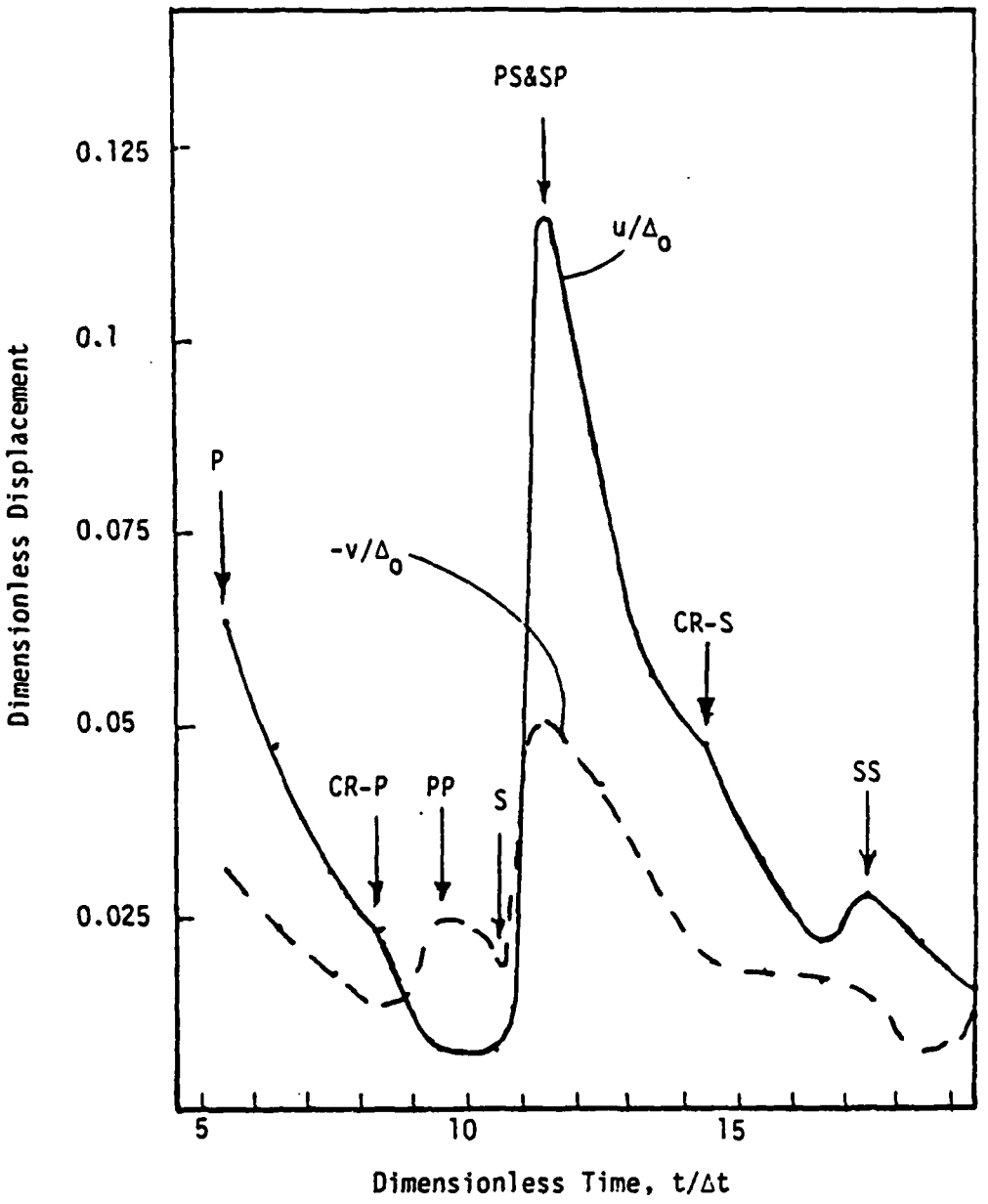

Fig. 6.13 Plane Strain Displacement Response at (0,5)cm.

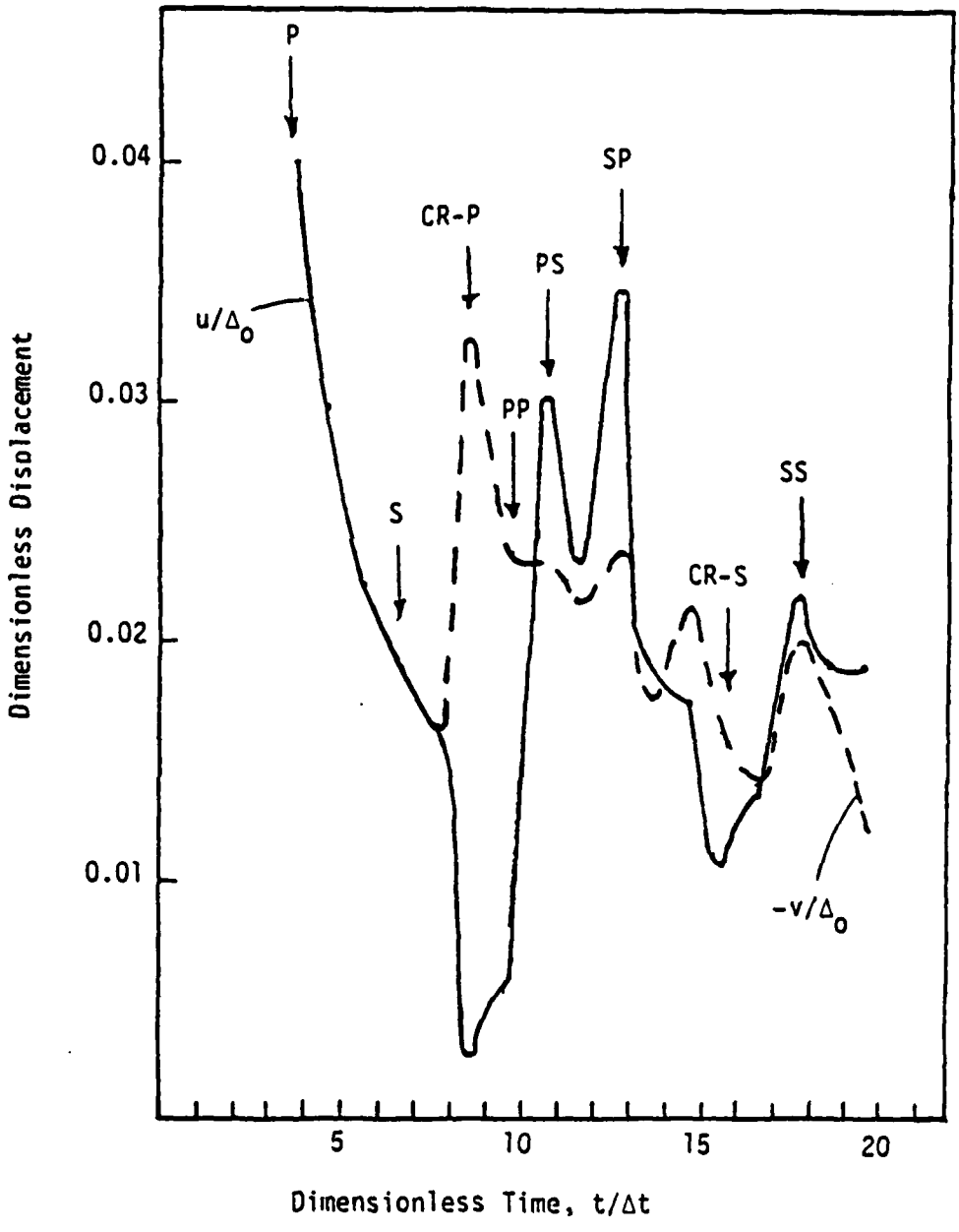

Fig. 6.14 Plane Strain Displacement Response at (-5,5)cm.

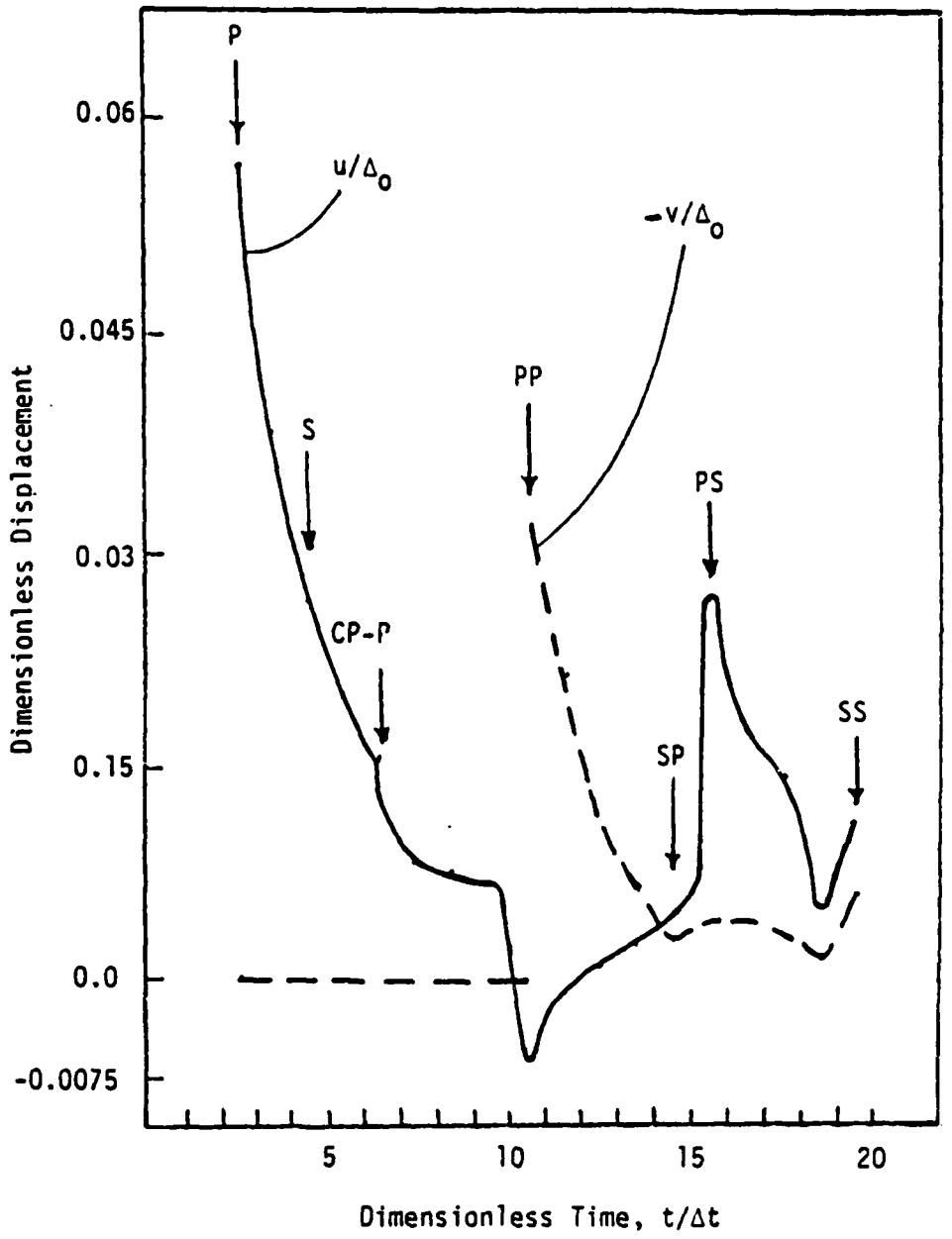

Fig. 6.15 Plane Strain Displacement Response at (-5,10)cm.

VII CONCLUSIONS AND RECOMMENDATIONS

This research focused on the feasibility of using a half-space, time-dependent Green's function as a fundamental solution for the construction of a direct BEM code to solve half-space wave propagation problems for in-plane and out-of-plane motions. With this half-space Green's function, the need to discretize the free surface was eliminated. The time dependent approach used here allows the causality principle to reduce the number of required computations and permits an explicit time stepping scheme to be constructed.

The present state of the method and code has some limitations and disadvantages. Since all previous time steps are required for the solution, large amounts of computer storage are necessary to use the methods developed. Another disadvantage is that while the method is good for transient problems, application to the steady-state harmonic problem reveals solution error propagation. This is due to the large number of time steps required and the need of all information from the previous time steps. Errors in the method arise from integrating the Green's function over its singularity. The steady-state harmonic problems have been successfully solved using BEM with Laplace and Fourier transform methods.

The example problem containing a buried source and a stress free circular cavity was modeled for both out-of-plane and in-plane motions. For this problem one can see the effect of a much more complicated wave phenomena for the in-plane (plane strain) case when compared to the SH-wave case. This is due to the effect of the free surface as it provides mode coversions of incident P- or SV-waves. Because of these

complexities, the time to compute a typical run was considerably longer for the plane strain problem.

This great increase in computation time over the SH-wave case is due in part to the complex nature of the Green's function. To solve for its values for a typical source/receiver pair, a Newton iterative root finding method must be employed (as explained in section 4.3). The root finding scheme is also used to find the ray path distances as described in section 2.5. There is also a considerable increase in the number of components of the Green's function; from two for the anti-plane strain case to seven for the plane strain problem. In addition the integration itself is more time consuming for plane strain. In the anti-plane strain case, integration was carried out using a differencing scheme from Cole [14]. For plane strain a Gauss four point quadrature was used which means the Green's function is evaluated 16 times for each space increment and time step.

In general, the developed methods are more accurate if $\Delta t\ c_2$ is approximately equal to the largest cavity size. When $\Delta t\ c_2$ is less than the dimension of the largest cavity the solution suffers convergence problems with increasing time. It appears that each element should receive influence from each of the other elements on a continuous surface. Additional numerical experimentation is needed to more accurately assess this phenomena.

The results obtained here for these plane strain and anti-plane strain problems show that the BEM with a time-dependent, half-space Green's function is a viable method for elastodynamic half-space problems. However additional research is needed in order to develop the technique into highly efficient numerical codes. The method could be

extended to include other interpolation functions (linear, quadratic, etc.). Although Cole [14], has indicated that lower order functions would be best, explicit studies of this point should be made. Nonhomogeneous continuum problems (layered media) could be investigated. Specifically for the anti-plane strain case one could use more image sources to simulate multiple layers. Anisotropic or nonlinear continuum could also be investigated, using the general method developed, providing the half-space Green's function could be found. The computability of the Green's function is very important on the overall performance of the BEM. The current state of the code developed, could certainly be enhanced by further improvements of the plane strain Green's function.

VIII. CONTRACT PUBLICATIONS

1. "Theoretical Ground Motions Using the Boundary Element Method," Sadd, M.H. and Rice, J.M., Proceedings Fourth Sensor Technology Symposium, Waterways Experiment Station, Vicksburg, MS, 1983, (to appear).

2. "Propagation and Scattering of SH-Waves in Semi-Infinite Domains Using a Time Dependent Boundary Element Method", Rice, J.M. and Sadd, M.H., to appear in Journal of Applied Mechanics, also to be presented at the ASME Winter Annual Meeting, New Orleans, LA, December 1984.

3. "Elastodynamic Boundary Integral Equation Solutions to the Half Space Problem Using a Time Dependent Green's Function: SH-Waves", Rice, J.M. and Sadd, M.H., Twentieth Annual Society of Engineering Science Meeting, University of Delaware, 1983.

4. "A Note on Computing Elastodynamic Full Field Displacements Arising from Subsurface Singular Sources", Rice, J.M. and Sadd, M.H., Submitted to Mechanics Research Communications.

5. "In-Plane Ground Motions Using a Time Dependent Boundary Element Method", submitted to International Journal of Numerical & Analytical Methods in Geomechanics.

6. "Transient Dynamic Solutions of Some Half Space Problems by the Boundary Element Method", Ph.D. Thesis, J.M. Rice, University of Rhode Island, May 1984.

IX. PARTICIPATING SCIENTIFIC PERSONNEL

1. Dr. Martin H. Sadd, Principal Investigator.

2. John M. Rice, Ph.D. Graduate Student, Received his Ph.D. in May 1984.

3. Krishnaswamy Kumar, M.S. Graduate Student, Employed in Summer 1982.

BIBLIOGRAPHY

1. Abduljabbar, Z., Datta, S.K., and Shah, A.H., "Diffraction of Horizontally Polarized Shear Waves by Normal Edge Cracks in a Plate," J. Appl. Phys., Vol. 54, No. 2, 1983, pp. 461-472.

2. Achenbach, J.D., Wave Propagation in Elastic Solids, North Holland, Amsterdam, 1973.

3. Achenbach, J.D. and Brind, R.J., "Scattering of Surface Waves by a Sub-Surface Crack," J. Sound and Vib., Vol. 76, 1981, pp. 43-56.

4. Achenbach, J.D., Gautesen, A.K., and McMaken, H., Ray Methods for Waves in Elastic Solids, Pitman, London, 1982.

5. Alder, B., Fernbach, S., and Rotenberg, M., Methods in Computational Physics, "Seismology: Surface Waves and Earth Oscillations," Vol. II, "Seismology: Body Waves and Sources, Vol. 2, Academic Press, N.Y., 1972.

6. Banerjee, P.K. and Butterfield, R., Boundary Element Methods in Engineering Science, McGraw-Hill, England, 1981.

7. Berezin, I.S. and Zhidkov, N.P., Computing Methods, Pergamon Press, New York, 1965.

8. Bouchon, M. and K. Aki, "Discrete Wave-Number Representation of Seismic-Source Wave Fields", Bull. Seism. Soc. Amer., Vol. 67, p. 257, 1977.

9. Bouchon, M., "The Importance of the Surface or Interface P-Wave in Near-Earthquake Studies", Bull. Seism. Soc. Amer., Vol. 68, p. 1293, 1978.

10. Bouchon, M., "Discrete Wave Number Representation of Elastic Wave Fields in Three-Space Dimensions", J. Geophys. Res., Vol. 84, p. 3609, 1979.

11. Brebbia, C.A., The Boundary Element Method for Engineers, Halsted Press, New York, 1978.

12. Brebbia, C.A. and Walker, S., Boundary Element Techniques in Engineering, Newnes-Butterworths, London, 1980.

13. Cagniard, L., Reflection and Refraction of Progressive Seismic Waves, McGraw-Hill, New York, 1962.

14. Cole, D.M., "A Numerical Boundary Integral Equation Method for Transient Motion," Doctoral Dissertation, California Institute of Technology, Pasadena, Calif., 1980.

15. Cole, D.M., Kosloff, D.D., and Minster, J.B., "A Numerical Boundary Integral Equation Method for Elastodynamics I," Bull. Seism. Soc. Amer., Vol. 68, 1978, pp. 1331-1357.

16. Cruse, T.A., "A Direct Formulation and Numerical Solution of the General Transient Elastodynamic Problem II," J. Math. Anal. Appl., Vol. 22, 1968, pp. 341-355.

17. Cruse, T.A. and Rizzo, F.J., "A Direct Formulation and Numerical Solution of the General Transient Elastodynamic Problem I,", J. Math. Anal. Appl., Vol. 22, 1968, pp. 244-259.

18. Datta, S.K. and El-Akily, N., "Diffraction of Elastic Waves in a Half-Space 1: Integral Representation and Matched Asymptotic Expansions," Modern Problems in Elastic Waves, Miklowitz, J., and Achenbach, J.D., ed., Wiley, New York, 1978, pp. 197-218.

19. de Hoop, A.T., "Representation Theorems for the Displacement in an Elastic Solid and their Application to Elasto-dynamic Diffraction Theory," Doctoral Dissertation, Tech. Hogesehole, Delft, 1958.

20. Eringen, A.C. and Suhubi, E.S., Elastodynamics, Academic Press, New York, 1975.

21. Ewing, W.M., Jardetsky, W.S., and Press, F., Elastic Waves in Layered Media, McGraw Hill, 1957.

22. Garvin, W.W., "Exact Transient Solution of the Buried Line Source Problem," Proc. Roy. Soc. London, Vol. 234A, 1956, pp. 528-541.

23. Graff, K.F., Wave Motion in Elastic Solids, Ohio State Univ. Press, 1974.

24. Hudson, J.A., The Excitation and Propagation of Elastic Waves, Cambridge University Press, Cambridge, 1980.

25. Kelly, K.R., Ward, R.W., Treilel, S., and Alford, R.M., "Synthetic Seismograms: A Finite Difference Approach," Geophysics, Vol. 41, Feb. 1976, pp. 2-27.

26. Ketter, R.L. and Sherwood, P.P., Modern Methods of Engineering Computation, McGraw-Hill, New York, 1969.

27. Kobayashi, S. and Nishimura, N., "Dynamic Analysis of Underground Structures by the Integral Equation Method," 4th International Conference on Numerical Methods in Geomechanics, Edmonton, Canada, 1982.

28. Kobayashi, S. and Nishimura, N., "Green's Tensors for Elastic Half-Spaces," Memoirs of the Faculty of Engineering", Vol. 42, Part 2, April 1980, pp. 228-241.

29. Kupradze, V.D., "Dynamic Problems in Elasticity," Vol. III, North-Holland, Amsterdam, 1963.

30. Lamb, H., "On the Propagation of Tremors Over the Surface of an Elastic Solid," Phil. Trans. R. Soc. London, A., Vol. 203, p. 1, 1904.

31. Manolis, G.D., "A Comparative Study on Three Boundary Element Method Approaches to Problems in Elastodynamics," Num. Meth. in Engineering, Vol. 19, 1983, pp. 73-91.

32. Mansur, W.J., and Brebbia, C.A., "Formulation of the Boundary Element Method for Transient Problems Governed by the Scalar Wave Equation," Appl. Math. Modelling, Vol. 6, August 1982, pp. 307-311.

33. Mansur, W.J. and Brebbia, C.A., "Numerical Implementation of the Boundary Element Method for Two Dimensional Transient Scalar Wave Propagation Problems," Appl. Math. Modelling, Vol. 6, August 1982, pp. 299-306.

34. Mendelsohn, D.A., Achenbach, J.D., and Kerr, L.M., "Scattering of Elastic Waves by a Surface-Breaking Crack," Wave Motion, Vol. 2, 1980, pp. 277-292.

35. Mendelson, A., "Boundary Integral Methods in Elasticity and Plasticity," NASA Tech. Note T.N.D.-7418, 173, 36 pp., 1973.

36. Mikhlin, S.G., An Advanced Course of Mathematical Physics, North-Holland, 1970.

37. Misljenovic, D.M., "Boundary Element Method and Wave Equation," Appl. Math. Modelling, Vol. 6, August 1982, pp. 205-208.

38. Misljenovic, D.M., "The Boundary Element Method in Shock Waves Analysis," Appl. Math. Modelling, Vol. 6, August 1982, pp. 312-315.

39. Niwa, Y., Kobayshi, S., and Azuma, N., "An Analysis of Transient Stresses Produced Around Cavities of Arbitrary Shape During the Passage of Travelling Waves," Memoirs Fac. Engng., Kyoto Univ., Vol. 37, Part 2, 1975, pp. 28-46.

40. Niwa, Y., Kobayshi, S., and Fukui, T., "Applications of Integral Equation Methods to Some Geomechanical Problem," Numerical Methods in Geomechanics, Desai, C.S., ed., ASCE, New York, 1976, pp. 120-131.

41. Payton, R.G., "Epicenter Motion of an Elastic Half-Space Due to Buried Stationary and Moving Line Sources," Int. J. Solids Structures, Vol. 4, 1968, pp. 287-300.

42. Reynolds, A.C., "Boundary Conditions for the Numerical Solution of Wave Propagation Problems," Geophysics, Vol. 43, 1978, pp. 1099-1110.

43. Rice, J.M. and Sadd, M.H., "A Note on Computing Elastodynamic Full Field Displacements Arising from Subsurface Singular Sources", submitted to Mechanics Research Communications.

44. Rice, J.M. and Sadd, M.H., "Propagation and Scattering of SH-Waves in Semi-Infinite Domains Using a Time Dependent Boundary Element Method," Journal of Applied Mechanics, to appear.

45. Rice, J.M., "Transient Dynamic Solutions of Some Half Space Problems by the Boundary Element Method", Ph.D. Thesis, University of Rhode Island, 1984.

46. Sanchez-Sesma, F.J., Herrera, I., and Aviles, J., "A Boundary Method for Elastic Wave Diffraction: Application to Scattering of SH-Waves by Surface Irregularities" Bull. Seism. Soc. of Amer., Vol. 72, pp. 473-490, 1982.

47. Shah, A.H., Wong, K.C., and Datta, S.K., "Diffraction of Plane SH-Waves in a Half-Space," Earthg. Engg. Str. Dyn., Vol. 10, 1982, pp. 519.

48. Shaw, R.P., "Boundary Integral Equation Methods Applied to Wave Problems," Developments in Boundary Element Methods-I, Applied Science Pub, London, 1979.

49. Sokolnikoff, I.S., Mathematical Theory of Elasticity, Second Edition, McGraw-Hill, New York, 1956.

50. Stone, S.F., Ghosh, M.L., and Mal, A.K., "Diffraction of Antiplane Shear Waves by an Edge Crack," J. Appl. Mech., Vol. 47, 1980, pp. 359-362.

51. Telles, J.C.F. and Brebbia, C.A., "Boundary Element Solution for Half-Plane Problems," Int. J. Solids Str., Vol. 7, 1981, pp. 1149-1158.

52. Wheeler, L.T. and Sternberg, E., "Some Theorems in Classical Elastodynamics," Arch. Rat. Mech. Anal., Vol. 31, 1968, pp. 51-90.

APPENDIX

COMPUTER PROGRAMS: BASIC STRUCTURE

Anti-Plane Strain Case

Figure A.1 illustrates the flow chart for the anti-plane strain program. The following are descriptions of the contents of the main program and subroutines.

MAIN PROGRAM: Calls three subroutines IMPUT,FMAT, and INTER.

IMPUT: Calls and defines all the variables necessary to solve the problem from a data file. These variables are the number and coordinates of the boundary elements on all cavities, number of cavities, the boundary conditions on each element, and the number and coordinates of the internal points at which a solution is desired. Also defined are the shear wave speed, shear modulus, the time increment, and number of time steps.

FMAT: Calls subroutine GF which will integrate the individual kernels for displacement and traction. FMAT also calls subroutine KOD which will provide the boundary conditions at each time step. A system of simultaneous linear algebraic equations are then formed from these integrated kernels and known boundary conditions. The unknown boundary conditions are next solved for by the simultaneous equation solver subroutine SLNPD using Gauss elimination. Finally subroutine STORE is called which stores the displacement and traction history for all surface elements.

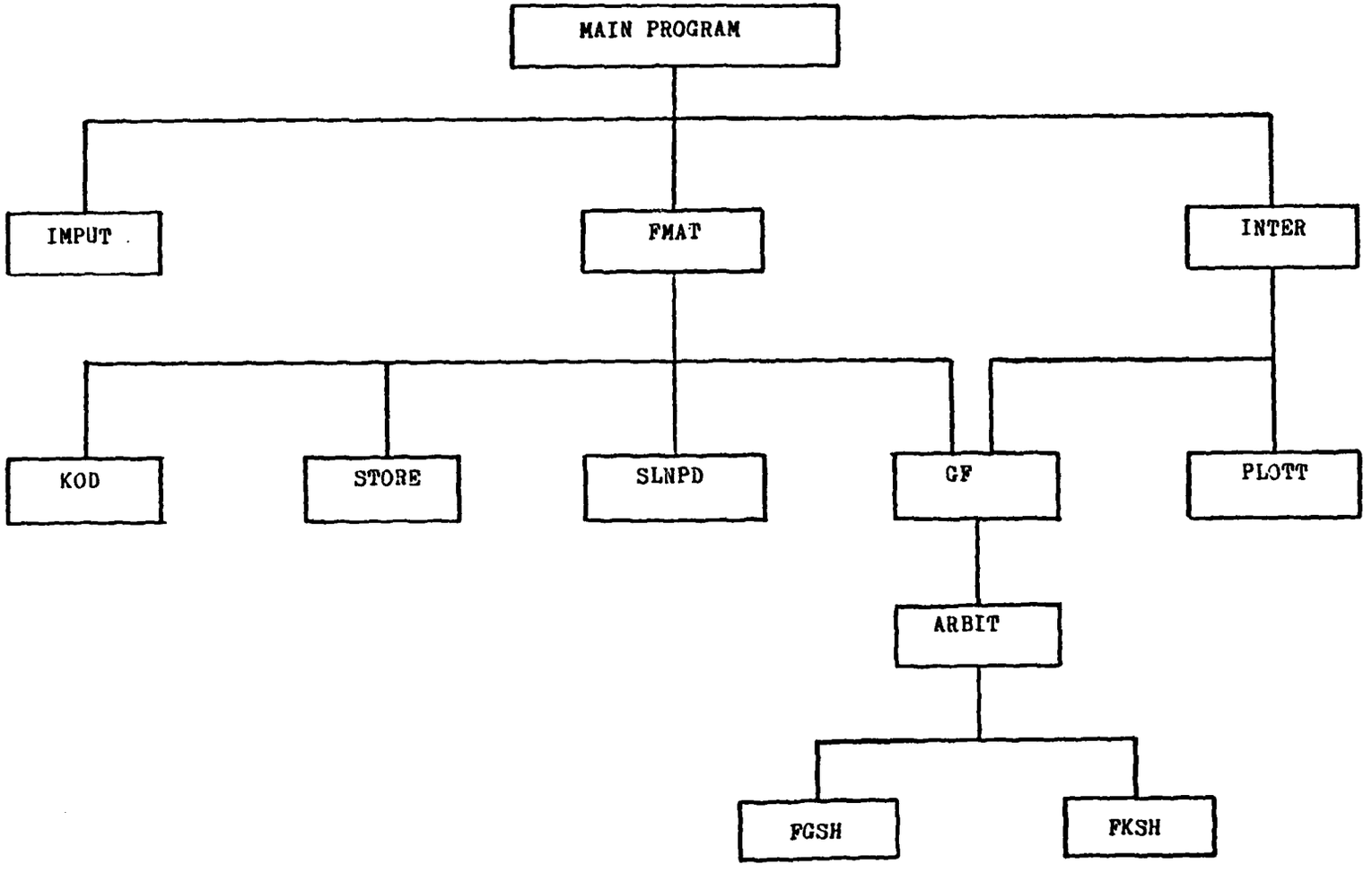

Fig. A.1 Anti-Plane Strain Program Structure

GF: Integrates the kernels using subroutines ARBIT, FGSH, and FKSH which are all given in detail in Cole [14].

INTER: Calculates the displacement at any point in the field except cavity surfaces.

PLOTT: Plots the displacement vs. time for the field points discussed in subroutine INTER.

Plane Strain Case

Figure A.2 shows the flow chart for the plane strain program. The following are descriptions of the contents of the main program and subroutines.

MAIN PROGRAM: Calls three subroutines IMPUT, FMAT, and INTER.

IMPUT: Calls and defines all the variables necessary to solve the problem from a data file. These variables are the number and coordinates of the boundary elements on all cavities, number of cavities, the boundary conditions on each element, and the number and coordinates of the internal points at which a solution is desired. Also defined are the mass density, shear wave speed, dilatation wave speed, the time increment, and number of time steps.

FMAT: Calls subroutine PSGF which will integrate the individual kernels for displacement and traction. FMAT also calls subroutine KOD which will provide the boundary conditions at each time step. A system of simultaneous linear algebraic equations are then formed from these integrated kernels and known boundary conditions. The unknown boundary conditions are next solved for by the simultaneous equation solver subroutine MATSOL using Gauss elimination. Finally subroutine STORE is called which stores the displacement and traction history for all surface elements.

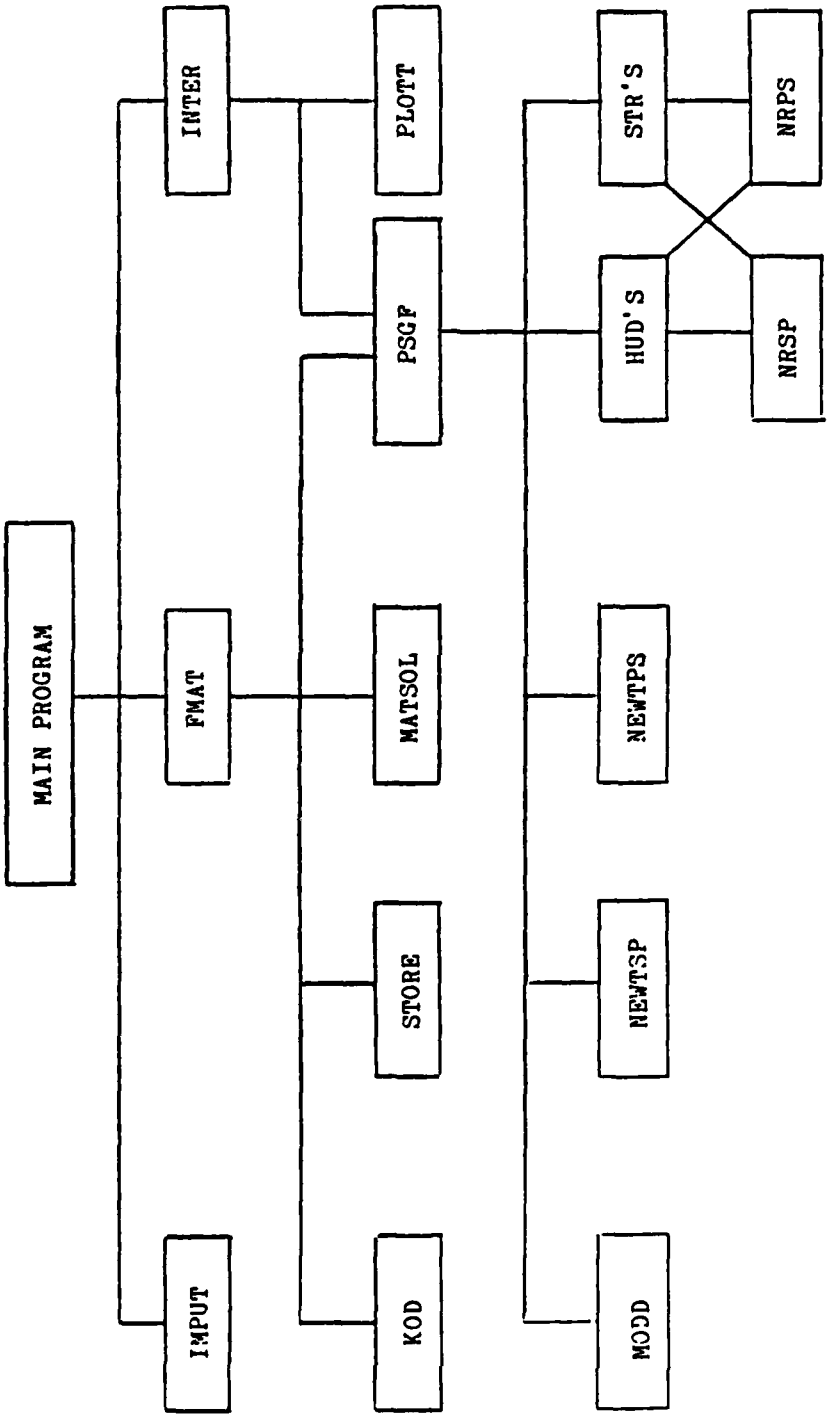

Fig. A.2 Plane Strain Program Structure

PSGF: Integrates the kernels containing the Green's function and associated stresses using a Gauss four point quadrature. If any Green's function does not decay properly after all the wave fronts have passed then subroutine MODD is called as a smoothing operation (as discussed in section 4.4).

HUD'S: HUD0,HUD1,HUD2,HUD3,HUD4, and HUD5 are subroutines that calculate individual components of the Green's function.

HUD0: Solves for the infinite space component.

HUD1: Solves for the PP component.

HUD2: Solves for the SP component.

HUD3: Solves for the PS component.

HUD4: Solves for the SS component.

HUD5: Solves for the SPS component.

STR'S: STR0,STR1,STR2,STR3,STR4, and STR5 are subroutines that calculate individual components of the stress associated with the Green's function.

STR0: Solves for the infinite space component.

STR1: Solves for the PP component.

STR2: Solves for the SP component.

STR3: Solves for the PS component.

STR4: Solves for the SS component.

STR5: Solves for the SPS component.

NRSP: Newton's method is employed to solve for the incident S-wave and reflected P-wave portion of the Green's function. This is accomplished by computing the roots of complex non-linear equations.

NRPS: Newton's method is employed to solve for the incident P-wave and reflected S-wave portion of the Green's function. This is accomplished by computing the roots of complex non-linear equations.

NEWTPS: Newton's method is used to evaluate the incident angle of a P-wave and the reflection angle of an S-wave, by obtaining the solution of two simultaneous non-linear equations.

NEWTSP: Newton's method is used to evaluate the incident angle of an S-wave and the reflection angle of a P-wave, by obtaining the soliution of two simultaneous non-linear equations.

INTER: Calculates the displacement at any point in the field except on cavity surfaces.

PLOTT: Plots the displacement vs. time for the field points discussed in subroutine INTER.

A complete listing of the computer programs may be obtained by writing to Dr. Martin H. Sadd, Department of Mechanical Engineering and Applied Mechanics, University of Rhode Island, Kingston, RI, 02881.

END

FILMED

10-84

DTIC